STRUCTURAL CONSIDERATIONS IN THE DEVELOPMENT OF POROUS MATERIALS

A Dissertation

by

ZACHARY PERRY

Submitted to the Office of Graduate and Professional Studies of
Texas A&M University
in partial fulfillment of the requirements for the degree of

DOCTOR OF PHILOSOPHY

Chair of Committee,	Hong-Cai Zhou
Committee Members,	Charles Culp
	Donald Darensbourg
	David Powers
Head of Department,	Simon North

August 2019

Major Subject: Chemistry

ABSTRACT

The study of porous materials dates back centuries to the discovery of activated charcoal used in holistic remedies across the globe. The recent advances in these materials has given rise to new applications and they sit a focal point of many energy related endeavors. This dissertation begins as an investigation of new materials for gas separations and storage and ends with a discussion on what structural considerations makes these materials function as they do. The need for new and improved methods for the capture and separation of carbon dioxide from air and energy emissions led to the development of a new cheaper benzimidazole based porous polymer network, PPN-101. This material demonstrated good surface area, 1095 m^2/g, and selectivity, 199 CO_2/N_2. The cost of this material and others is also discussed. The development of new porous cage based materials for hydrogen and methane storage were investigated. This resulted in the synthesis of five chromium(II) paddle wheel based cuboctahedral cages with a total of seven different structures due to multiple possible packing schemes were investigated. Utilizing 5-tert-butylisophthalic acid and chromium(II) acetate monohydrate a highly porous molecular cage based material was obtained with a BET surface area of over 1000 m^2/g. Difficulties in obtaining further structures and the presence of multiple packing modes observed for different ligands led to an analysis of the contributions solvents and surface functionalization provide these systems. An analysis of cage-solvent interactions resulted in identifying key interactions between ligands and coordinated solvents. Though no further new crystal systems were observed,

this resulted in the preliminary observation of the second non-axially coordinated chromium(II) carboxylate paddle wheel complex via solution state UV-Vis. These results indicate that porous materials can be achieved through molecular coordination compounds through judicious control of ligand interactions, geometry, and the strength of metal-metal interactions.

DEDICATION

To those that came before on whose shoulders I stand,

So long, and thanks for all the fish

ACKNOWLEDGEMENTS

I would like to thank my PI Joe Zhou for the mentorship and experiences he allowed me to have and the many enthusiastic conversations we've had over our chemistry, the lab, and science in general. In my time at Texas A&M I have worked with many fine researchers and I would like to thank a few of them for their specific contributions to my Ph.D. experience: Dr. Jinhee Park for several years of fruitful collaboration and mentorship, Dr. Julian Sculley for making sure I knew what I was doing when I first arrived and for frequent conversations on my work, Dr. Trevor Makal who was willing to tell it like it is and still provides sage advice, Dr. Jihye Park for many helpful conversations and mentorship in my initial time in graduate school, and Stephen Fordham for the laughs and BBQ he provided. I would also like to thank the host of younger graduate students in the Zhou group and in others who have stepped up and provided much assistance and comaradarie, specifically, Creg Day for his helpful chemistry insights and less so for his punishing sense of humor, Elizabeth Joseph, Hannah Drake, Jeremy Willman, Sayan Banerjee, and Angelo Kirchon.

One of the most lasting experiences of my graduate career was the ten weeks I spent at the National Academies of Sciences, Engineering and Medicine as a Christine Mirzayan Science and Technology Policy Fellow. My mentor Marilee Shelton-Davenport provided me with much insight and valuable connections and the program itself offered the kind

of hands on experience in the science policy ecosystem that one can only get in Washington, D.C.. If you are reading this, and are within 5 years of obtaining your graduate degree or still a student, think about applying to this or similar programs. No matter what your professional goals are the perspective gained will help you navigate science outside of the laboratory and in with a renewed appreciation for the process and the impacts you are creating.

I received by Bachelors of Science in Chemistry from the University of Tennessee at Chattanooga and the wonderful professors there provided me with the privilege of doing research that ultimately led to the drafting of this dissertation. Professors Gretchen Potts, Robert Mebane, John Lynch, Tom Rybolt, Jisook Kim, and John Lee provided me with an education in chemistry that stretched across disciplines and prepared me for my journey these past seven years. Jim Narramore provided me with stories to tell about chemical safety, in some of which I play a bit part, and operations of a chemistry lab that I will be telling for the rest of my life. However most important to my growth and indeed career as a researcher was Professor Greg Grant who gave me a chance to do summer research that resulted in trips to Honolulu, Richmond, Anaheim, San Diego, and all that followed in my time in College Station.

Lisa Logan my 9th grade physical science teacher managed to keep the class entertaining with tales of her masters research, injecting mice with THC to see if affected spatial perception, and engaged with all of the students regardless of their interests. Terri

Bicknell much as she tried could not keep my attention in biology, she was very good at her job I was not. Due to moving across the country and back I took way more high school chemistry, three credit years worth, than the typical student, from two teachers, one in Kansas who taught a comprehensive and thought provoking class and one in Georgia who taught me to evaluate science communication critically as they did not believe in global warming or “macro”-evolution. Without their outspoken, and quite incorrect, interpretations of the facts I might have remained oblivious to the ignorance that can pervade even those who we expect to teach us. This counterintuitively inspired in me an interest in science communication and a certain civic duty in sharing the good word of good research.

I had one middle school science teacher Sandra Roebuck who kept us engaged with making cakes that looked like cells and experiments that we could relate too. She also mixed bleach and ammonia in the trashcan one time while throwing out the Dixie cups containing the unknowns from the previous class’s experiments. I noticed the rising vapors and exclaimed “it’s a chemical reaction”, I’ve always made the most astute of observations. She kept science and worked to make sure we all did eventually understand what she needed to teach us, it is an example I always try to follow.

My primary teachers all provided me with the resources I needed to learn Paula Crosby at Graysville Elementary most of all.

My brothers Will and Josh have graduated both high school and college while I've been here and are past the point where they need my help with homework but now I can return the favor as them about life after school.

My grandfathers Papa Jim and Papa, a chemist and an engineer, helped spark my appreciation for science and have always provided support when I needed it. My grandmothers Mamas Judy and Sue also provided plenty of topics to discuss and learn especially encouraging a love of reading from a young age. My aunts and uncles have all supported me and provided me with books that have served as a welcome distraction from time to time.

And finally I would like to thank my parents Bill and Gretchen who have provided me with all I ever needed and put up with me all these years. My mom always had the food network on and some of my earliest science engagement was with Good Eats. So I'd like to thank two A.B.s one for teaching me how cooking food works and the other for helping me to understand the broader picture how food and society are intertwined.

All of these people and more that I've surely forgotten have provided me with privileges that touch on almost every level of my life and I can't thank them enough for what they have done for me or how it has enabled me to be where I am today.

CONTRIBUTORS AND FUNDING SOURCES

Contributors

This work was supervised by a dissertation committee consisting of Professor Joe Zhou the Department of Chemistry and Professor(s) Charles Culp of the Department of Architecture and Professors Donald Darensbourg and David Powers of the Department of Chemistry.

The work in Chapter 2 was conducted in part by Dr. Muwei Zhang of the Department of Chemistry and was published in 2014. The work in Chapter 3 was conducted in part by Dr. Jinhee Park of the Department of Chemistry. Dr. Park solved the crystal structures published in 2017 of the first three chromium cage compounds and along with J. Bae collected the powder patterns of Cr-1 and Cr-3. These structures were also used in the structural analysis in Chapter 4.

All other work completed for the dissertation was completed by the student independently.

Funding Sources

Graduate study was supported in part by a teaching assistanceship from Texas A&M. This work was supported as part of the Center for Gas Separations, an Energy Frontier Research Center funded by the U.S. Department of Energy, Office of Science, Basic Energy Sciences under Award # DESC0001015 (CO_2 separations and initial MOP studies), and the Welch foundation under grant A0030 (additional supplies and salary

support). Its contents are solely the responsibility of the authors and do not necessarily represent the official views of the Department of Energy or the Welch Foundation.

TABLE OF CONTENTS

Page

LIST OF FIGURES

Page

LIST OF TABLES

Page

CHAPTER I

INTRODUCTION

1.1 Porous Materials and their Uses

Porous materials based on coordination structures and organic polymers have over the past two decades advanced into one of the fastest growing areas of chemistry and material science.[1-4] This has been due to the realized tunable nature and far reaching applications of highly porous materials such as gas storage, separations, catalysis, medical diagnostics, and therapeutics.[5-10] This dissertation will focus on discrete factors that enable porosity and improve performance towards possible applications of these materials.

1.1.1 Highly Porous Materials

Highly porous materials are those with high surface areas and accessible interior pore volumes. These are categorized into several well studied areas activated carbons, zeolites, porous polymer networks (PPNs), [3, 11-13] metal-organic frameworks(MOFs), [14-16] and more recently metal-organic polyhedra (MOPs).[17-18] These materials all have distinct advantages and disadvantages in their application toward gas adsorption and separations. The materials under study in this dissertation fall into the categories of porous polymer networks and MOPs.

1.1.1.2 Porous Polymer Networks

Porous polymer networks are materials composed entirely of covalent bonds between organic and main-group structural units. These units are typically rigid and provide some steric or directional control to the synthesis. PPNs range from highly ordered crystalline organic frameworks (COFs), [19] to completely amorphous polymers[20] but the defining feature is that they have a measurable porosity once activated by removing solvent within pores in the structure. They may have inherent functionality such as *N*-donor groups[21] or be functionalized post-synthetically to included desired moieties[22]. Due to the robust nature of these covalent bonds these materials have high chemical and thermal stabilities and as such are of great interest in applications where other materials often foul or decompose.[3, 12, 23] More specifics about PPNs and their use in carbon capture is discussed in Chapter II.

1.1.1.3 Metal-Organic Polyhedra

The coordination chemistry of metal ions bound by organic ligands has a rich history concerning both discrete molecular complexes and extended polymeric materials.[24-25] The discovery of metal-organic frameworks (MOFs) in the early 1990s and realization of their high permanent porosity provided an all new avenue for this field of research.[26-27] MOFs are generally defined as coordination polymers that extend in a regularly

repeating fashion in three dimensions and have potential or measured porosity.[28] Coordination polymers had been well-studied but the relatively recent realization that some of these systems could maintain porosity after removal of solvents has quickly garnered attention.[16]

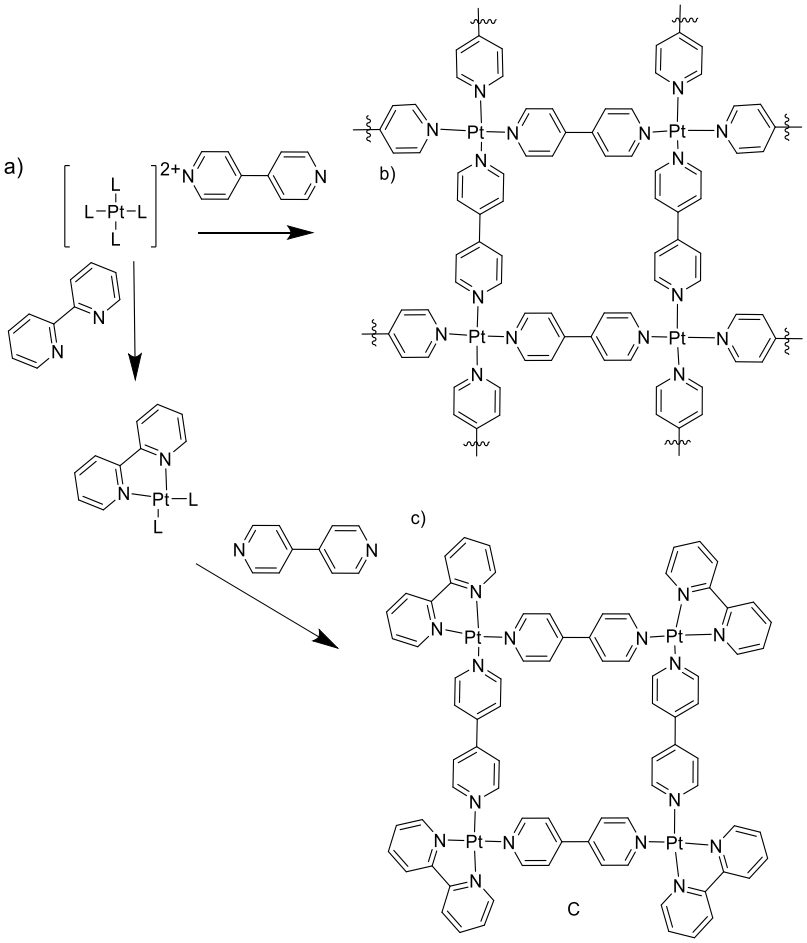

Figure 1 The two pathways for preparation of capped precursor and square (down) vs. the direct assembly of infinite coordination right. Coordination polymer b extends indefinitely along the plane of the paper while c exists as a molecular species.

Almost immediately, MOFs were seen as a replacement for zeolites in many applications for porous materials. This includes heterogeneous catalysis, separations, and perhaps most ubiquitously for the capture and storage of strategic gasses. However, another class of materials also arose during this time period, MOPs.[25, 29-31] MOPs share many of the same characteristics and even structural moieties as MOFs; however, they lack bridging between the individual cages which leads to some inherent complications for their applications in solid state chemistry. Metal-organic polyhedra are discrete cages formed from the bridging of metal centers by organic ligands via coordination bonds. Geometrically, MOPs and MOFs differ in the connectivity, convergent versus divergent, of their two components, metal node and linker. For a coordination polymer to be produced the symmetry and connectivity of these two elements must be such that an infinite number can be added to the initial coordination complex (Figure 1b). MOPs on the other hand, require the geometry to be convergent, such that when the symmetry of the node and ligand are combined the resulting polymer meets itself and closes rather than infinitely repeating (Figure 1c). In fact for the two examples, Figure 1 b and c, the empirical formula, $C_{20}H_{16}N_4Pt$, is identical and the coordination environment around the platinum is essentially the same; however, convergence is obtained via the capping of the platinum center. This is intuitive as we know that a square has four linear sides and four 90 degree corners. The 4,4'-bipyridine acts as the linear side while the 2,2'-bipyridine capped Pt(II) acts as the vertices. There is also a logical extension of these into the third dimension if we consider an octahedral metal coordination environment. With six divergent linear linkers (4,4'-bipyrdine) an infinite network of vertex shared

cubes is formed. However if the metal is capped facially the resulting trigonal pyramidal node gives a cubic cage. In theory, any polyhedron could be produced as a MOP if the geometry of the vertices and ligands can be matched synthetically.[17, 32] So long as a suitable way to reduce the connectivity of a given node is found, reduction of a polymeric framework to its constituent building blocks can be realized. Though this is not always feasible given the realities of synthesis. Such coordination assemblies have been synthesized from a wide variety of metals and ligands yielding a large number of geometries and functionalities.

The first carboxylate-bridged MOP, copper isophthalate, was published by the Yaghi group and paved the way for much of the current research.[33] The Zhou group has worked on the synthesis of a wide variety of cages and developed several methods for predicting structure and properties of these systems. The main connectivity in these cages is provided by $M_2(RC(O)O)_4$ paddlewheels, principally copper, molybdenum, and in most recently chromium.[17, 29, 34-40] The group has developed several methods for structural and functional control via bridging angle, ligand substitution, surface functionalization, and intermolecular directing forces[35, 39, 41-42]. Though MOPs seem at first glance seem to possess inherent porosity due to their internal pores, little work has been done studying such systems as few studies showed promising results.[43-45]

MOPs being porous molecular cages means that they do not often maintain their crystalline order after removal of solvent and impurities as intercage interactions are

often weak. This is because of three factors: 1) the solvents and other molecules may play a role in the packing forces leading to disorder and aggregation when removed, 2) inherent packing motif may cause windows to be blocked, limiting solvent diffusion through the resulting material and 3) the harsh conditions of the activation process such as elevated temperatures and high vacuum can result in cage disorder or collapse as the metal ligand interactions are ruptured or reorganized. As such only a handful of cases of MOPs have been reported as retaining some high level of porosity suitable for gas applications in materials without strong interactions bridging the cages.[41, 46-50] This lead to the investigation of chromium(II based) MOPs, due to the metal-metal bonding within the paddle wheels, as porous materials which were first successfully reported by the Zhou group and shortly thereafter by the Bloch group in 2017.[47]

1.2 Basic principles of gas sorption

1.2.1 The pore and the isotherm

As the defining feature of porous materials is the presence of a measurable pore volume a system of conventions has been developed to formalize how we discuss them. IUPAC has developed recommendations for the different types of adsorption isotherms observed in these materials (Figure 2). These are representative of the pore environment within the material. Type I isotherms exhibit a steep initial rise in adsorption and then plateau until saturation is reached. This indicates micropores, pores less than 20 Å, are present in the

interior of the material. Type II isotherms have an initial rise after which they plateau and then have a point of inflection while the isotherm rises to saturation pressure. This indicates the material contains macropores (pores > 500 Å) as indicated by the low uptake at low pressures and increasing uptake at higher pressures. Type IV isotherms

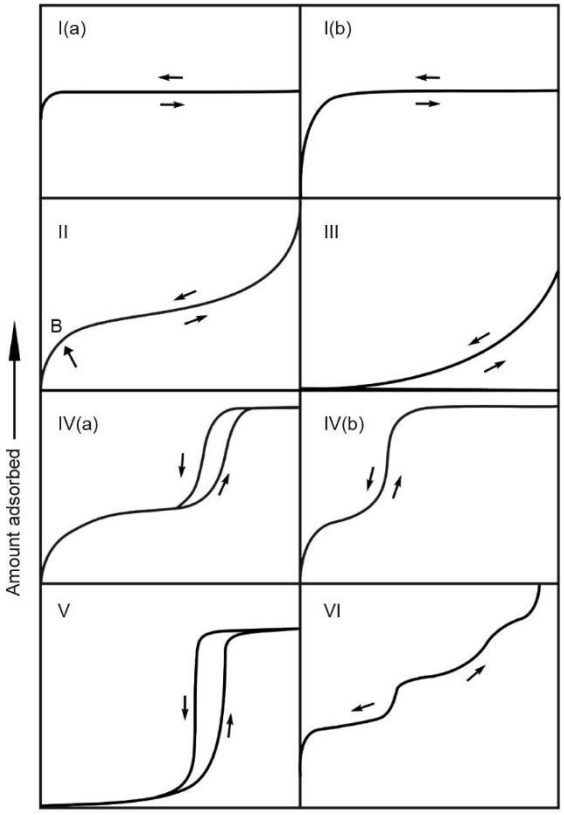

Figure 2 IUPAC isotherm types[51]

indicate that some mesopores of a specific range are present in the material but no macropores (> 20 Å and < 500 Å) as there is no additional adsorption at high pressures.

These help categorize materials based on their gas uptake from visual inspection of the isotherms.

1.2.2 Quantifying surface area and porosity

Perhaps the most compared characterization value for porous materials is the surface area. Two models are often used in the literature the Langmuir and BET theory models. The Langmuir model is quite simple and makes several assumptions that make it a poor choice for microporous materials. It assumes a perfectly flat surface covered in a single layer by the adsorbate with equivalent adsorption sites through the entire material. While this model works for materials that have little internal porosity or very large pores it does not apply well to microporous materials like those discussed in this dissertation.[51] The Brunauer–Emmett–Teller method thus will be used in this dissertation. There is some concern about this model as well, however it is the standard by which all other materials are compared.[51-52] The concerns arise from the nature of the BET equation where the presence of multiple adsorption sites who's sorbate condensation overlaps in the microporous region of the isotherm. However DFT methods have not been standardized making the BET method the best method for comparison of similar materials.

BET theory assumes a multi-layer model of gas adsorption wherein additional layers of sorbate can adsorb to the initial layer on the surface of the sorbent.[52] This makes it a better model than the Langmuir model for estimating the surface area of microporous solids.

$$\frac{P/P_0}{n(1-P/P_0)} = \frac{1}{n_m C} + \frac{C-1}{n_m C}(P/P_0)$$

Equation 1 BET Equation n is moles of gas adsorpbed at pressure P/P_0 and C is the BET constant

The BET constant is obtained through a transformation of the measured isotherm by selecting points in a range of 0.05 to 0.3 P/P_0 where the plot is linear. This is typically derived via the instrument software with the points for analysis being selected manually.

CHAPTER II

COST-EFFECTIVE CARBON CAPTURE BY A POROUS POLYMER NETWORK*

2.1 Introduction

2.1.1 The Carbon Dioxide Separations Problem

Carbon dioxide contributes to many factors in the global environment and anthropologic sources are attributed with inducing worldwide effects including acidification of the oceans and global warming.[53] These changes threaten both the environment and humanity with a permanent change if nothing is done to curb these emissions. It is widely recognized that removing carbon dioxide from the air and industrial waste streams is necessary in combating global warming and climate change.[53] To combat the continued rise of global carbon dioxide emissions the area of Carbon Capture and Sequestration (CCS) has developed to create a system to reduce, remove, and remediate carbon emissions from anthropologic sources.[54] Traditional systems that have been used for decades such as monoethanolamine solutions have good raw performance numbers for selectivity and uptake of CO_2 from waste streams and together with other alkanolamine derivatives make up the current industrial state of the art carbon dioxide removal systems.[10] However the

*Part of the data in this chapter is reprinted and adapted with permission from Zhang, M. W.; Perry, Z.; Park, J.; Zhou, H. C., Stable benzimidazole-incorporated porous polymer network for carbon capture with high efficiency and low cost. *Polymer* **2014,** *55* (1), 335-339 Copyright Elsevier 2014.

current limitations of these systems make them impractical for widespread implementation in an efficient and cost-effective manner.[20] This includes their environmental toxicity, corrosivity, and high regeneration costs due to the energy requirements needed to release the CO_2 trapped in the solutions. Alkanolamine solutions traditionally have required as much as 30% of a power plant's output for operations that capture 90-100% of CO_2 emitted.[55] In practical terms a large portion of extra hydrocarbons must be consumed to generate the energy necessary to capture the base level of CO_2 as well as that energy expended in the carbon capture process.

2.1.2 Solid Sorbents for Carbon Capture

To reduce the negative aspects of carbon capture processes, solid sorbents have become a focus of research in the area. Due to their solid nature they are more easily contained and do not readily react with the materials that constitute the carbon capture system. Additionally, by reducing the mass of material that does not play a role in carbon capture, such as the water in aqueous alkanolamine solutions, the total energy requirements for such systems can be lowered significantly over solution-based methods. The rapid development of these materials since the early 1990s[1] has spurred a wide swath of new research areas under the promise of highly-tunable molecular designs enabled in these new systems.[56] In the classes of advanced porous materials outlined in Chapter 1 researchers have found the potential to solve the current limitations through the use of metal-organic frameworks (MOFs)[57] and porous polymer networks (PPNs)[13] as they represent the most

promising materials in the area of adsorption based[13, 58], gas separation[48, 59] owing to their high surface areas and broad design possibilities. Traditionally MOFs provided a trade-off in material tunability and structural variety with poor stability under practical conditions for carbon capture as well as high synthetic costs.[11] Stability is of lesser concern in newer generations of MOF materials, however, these often do not show the high gravimetric capacity of other materials. Stability is however an area of lesser concern in newer MOF systems though carbon capture performance is most systems is[3, 60] not adequate in such systems.[61] As an alternative PPNs, owing to their construction largely from C-C, C-O, and/or C-N bonds, have physical properties such as increased stability and lower mass/unit volume that are desirable in post-combustion carbon capture systems.[62] Crystaline organic Frameworks (COFs)[19] alternatively span the divide between the long-range order of MOFs and the amorphous nature of PPNs. COFs are often fragile and many early systems, such as boronic ester COFs, lack the stability of PPNs. With Brunauer–Emmett–Teller (BET) surface areas as high as 6461 m^2/g (in PPN-4), PPNs have the potential to be some of the most porous materials known.[13] However impressive surface area and other characteristics do not yield increased CO_2 capture performance in the same way gasses such as methane and hydrogen are generally improved. This is due to the fact that hydrogen and methane storage/separation systems rely on weak physisorptive interactions rather than the chemisorptive systems found most practical for CO_2.

It is important to understand a typical post-combustion flue gas system to see how the

limitations of many materials render them implausible for implementation (Fig 1). Perhaps most important is understanding the composition of flue gas which is the waste stream coming from a hydrocarbon burning power plant. It is this flow of gas that is scrubbed of CO_2 but also what provides the difficulties over what is typically studied in the lab. This gas stream is scrubbed of the bulk of sulfur oxides, nitrogen oxides, and other acid gases before being sent through the CO_2 scrubbing column. While typical lab and bench-scale testing is performed in stationary phase systems current state of the art systems utilize fluidized beds to maximize contact between sorbent, such as aqueous alkanolamine, and the gas stream. The final gas stream thus consists of 12-15% CO_2, 12% H_2O, 4% O_2, and the remainder largely N_2 with minor sulfur oxides and nitrogen oxides at <100 ppm levels.[3]

2.1.2.1 Porous Polymer Networks for Carbon Dioxide Capture and Separations

Previously some of the most promising PPNs developed in the Zhou lab, the PPN-4 and PPN-6 families, had synthesis regimes that were not compatible with scale-up to commercial systems. The costly Yamamoto homo-coupling reaction[62] requires bis(cyclooctadiene)nickel ($Ni(cod)_2$) as a stoichiometric reagent as well as greater than stoichiometric amounts of cyclooctadiene to yield the best materials. At scale, this is a significant barrier. Further, these materials, while having remarkable surface areas, have no functionalities that can adequately bind CO_2. This relegates the base material to only physisorption which cannot yield a high enough CO_2 capacity for practical applications. In order to effectively serve in a non-physisorptive capacity such systems must undergo

post-synthetic chemical modification (PSM) to install appropriate functional groups;[20, 63] there is however a delicate balance as PSM increases affinity for species of interest it also decreases porosity. It is highly desirable to synthesize functionalized PPNs with considerably large porosities and reasonable production costs for industrial CCS processes.

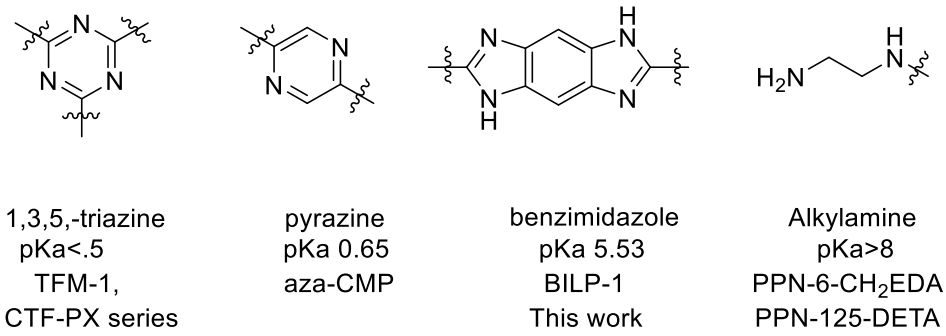

Figure 3 pKas of common nitrogen containing moieties in PPNs

It has been well established that inclusion of lewis basic moieties within MOFs[60, 64]and PPNs[20, 22, 65-66] CO_2 capacity and CO_2/N_2 selectivity can be increased. There are several options of inclusion of such sites either through direct incorporation into the backbone, post-synthetic modification which fixes the basic moieties to the PPN backbone, or simple loading of the pores with basic-nitrogen containing species.[3]

Several types of *N*-donor moieties have been incorporated into PPNs including triazine, [67-68] cyclic amides and alkyl amines,[66] pyrazine,[69] and polyamines.[20] However it is typically seen that the higher material performance observed the higher the synthetic cost

for the material. Triazine moieties typically show poor selectivity as shown in TFM-1[67] and CTF-PX series[68] due to the poorly basic nature of the triazine moiety.

In contrast, the fixing of polyamines into PPNs[20, 22, 65] has been demonstrated as an efficient way to improve the CO_2/N_2 selectivity. Though the performance metrics of many of these materials are promising in a vacuum they do not hold up to the rigors required by CCS systems. To try to bypass these issues a new material PPN-101 was synthesized. This material contains benzimidazole units which serve as the CO_2 binding sites while also serving as part of the rigid backbone of the material. At the time of publication the synthetic pathway a cost-effective material as compared to those published previously.[21]

2.2 Results and Discussion

To accomplish the synthesis of a rigid basic PPN the condensation of the tetrahedral monomer tetra-4-carboxyphenyl silane with 1,2,4,5-tetraamino benzene followed by oxidation gave PPN-101 with a theoretical diamonoid net (Figure 4).

Materials based on polybenzimidazoles have been utilized in the area of proton conduction, however, what makes a material good for proton conduction does not translate to good CO_2 capture performance.[70] This is because for proton conduction it is ideal to limit the distance between donor sites whereas in any adsorptive application it is porosity that is desired. Previous to this work a PPN, BILP-1 (Benzimidazole Linked Polymer) was published by Kalderi utilizing the of tetrakis(4-formylphenyl)methane and

2,3,6,7,10,11-hexaaminotriphenylene. This material has a 1172 m^2/g BET surface area and 18 wt% CO_2 loading capacity at 273 K and 1 bar.[71] The bulky aromatic amine and carbon centered monomers however limited practicality of this material as their costly

Figure 4 Tetrahedral node and linear linker that comprise the theoretical diamondoid net of PPN-101.[21]

multi-step syntheses are not cost-effective or practical at scale for CO_2 capture.[72] [73] PPN-101 alternatively uses a simple synthesis for the silicon-centered tetrahedral monomer[74] and the commercially available 1,2,4,5-tetraaminobenzene was chosen for the bridging monomer (Figure 5).

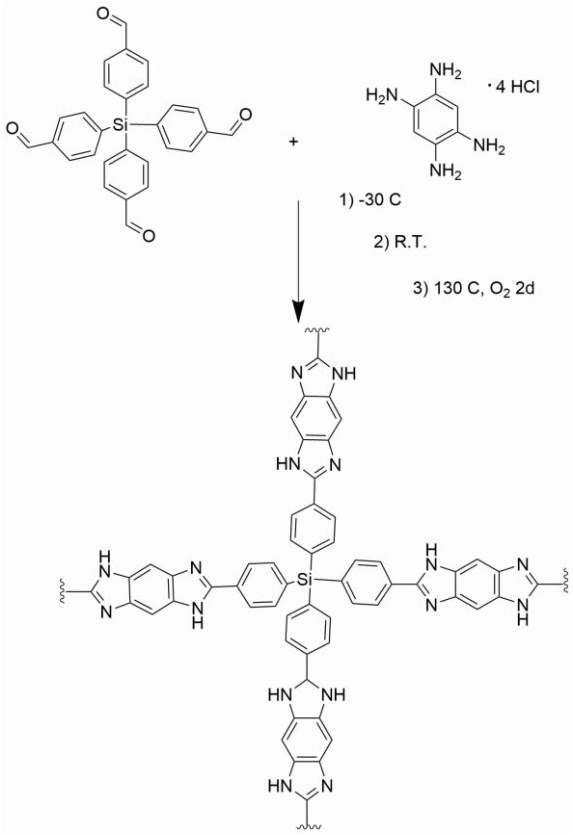

Figure 5 Synthesis of PPN-101

2.2.1 Preparation and Structure of PPN-101

The tetrahedral geometry was chosen due to the relatively small pore size(~14 Å) and the literature trend of good performance for tetrahedrally centered PPNs.[11, 13, 62] The diamondoid topology arises from an ideal orientation of tetrahedral and linear monomer units. This allows for a high connectivity, which helps support the framework, as well as ensuring accessibility of the benzimidazole moieties within the pore volume.[62] The diamond topology also limits interpenetration enabling a higher percentage of the benzimidazoles to be accessible in the synthesized PPN.[13] The silicon centered monomer

has a more facile synthesis contributing to the overall potential cost reductions.[15]

The polymer was synthesized by adding 2 eq. of tetraaminobenzene monomer to a chilled, 30 °C, solution of the tetrahedral monomer in DMF. An orange precipate formed and the reaction was allowed to rise to room temperature overnight. To complete the reaction the flask was purged with oxygen gas and heated to 130 ˚C and kept at this near reflux condition for two days. It must be stressed that DMF is a flammable solvent and that great care must be taken during this step. Use of a blast shield and temperature probe controlled heating bath are necessary safety precautions. The resultant yellow solid was centrifuged from the supernatant and dried under vacuum giving a 59% yield.

2.2.2 Porosity and CO_2 Adsorption in PPN-101

The observed porosity of PPN-101 indicated that study of its gas uptake properties was feasible. The sharp type-I 77 k N_2 isotherm (Fig. 7) indicates microporosity within the sample as expected based on the distance between the tetrahedral centers of ~18 Å and a distance across the tetrahedral pore, from vertex to face, of ~17 Å. The BET surface area of 1095 m^2/g and pore volume of 0.66 cm^3/g are reasonable for the expected structure. The pore-size distribution was obtained using the Density Functional Theory (DFT) method in the instrument software (Figure 6 (b)). The broad distribution of pore sizes from 12 Å to 35 Å fit well with the calculated pore size, allowing for defects involving one to two pores. The material itself, however, shows no regular order as seen by the powder x-

ray diffraction pattern which is defined by a single broad feature that is assigned to solvent in the pores and the general amorphous nature of the solid. The most obvious pore

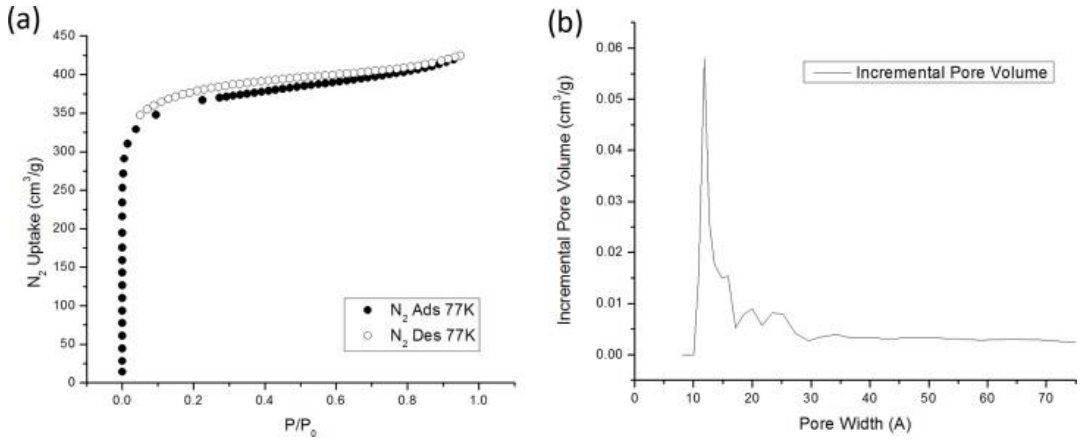

Figure 6 Porosity measurements of PPN-101 a) N2 isotherm at 77 K and b) incremental pore volume[21]

diameters are at 11, 16, and 19 Å, this is in line with both the observed micro-porosity and the estimated pore size. This is 2-3 times the observed pore size in the BILP-1 PPN.[71] This is attributed both to the bulky nature of the benzimidazole bridging groups and the diamondoid topology between monomer units.[13]

The high *N*-donor content as well as moderate surface area and pore volume provide good selectivity for this material. The isotherms of CO_2 at 273 K and 296 K and the N_2 isotherm at 273 K are shown in Figure 7(a). Carbon dioxide shows reversible adsorption with a maximum of 226.2 mg/g at 1.1 bar and 273K, significantly greater than the 188 mg/g for BILP-1.[71] This can be explained by the greater pore accessibility of PPN-101 and its higher

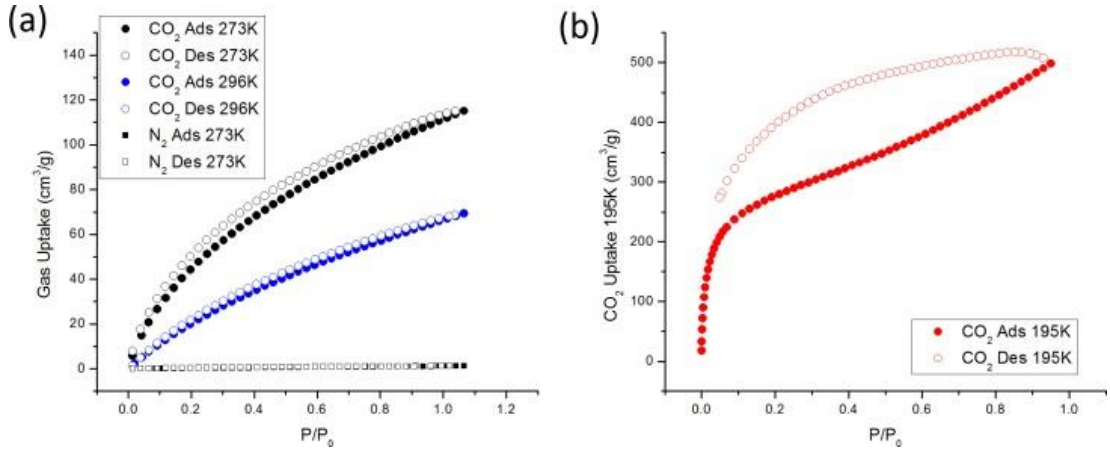

Figure 7 Carbon dioxide uptake and N_2 uptake for PPN-101[21]

nitrogen content, 17% vs. 14% by weight nitrogen. For comparison CO_2 uptake at 195 K and 0.95 bar the CO_2 uptake reaches 498 cm^3/g this is most comparable to the N_2 uptake values as these are near condensing conditions (Figure 7b).

2.2.3 CO_2/N_2 Selectivity of PPN-101

To calculate the selectivity for a theoretical flue gas of 15% CO_2 the values of CO_2 adsorption at 0.15 bar and N_2 0.85 bar adsorption at 273 K were used. The observed low N_2 value translates to a selectivity of 199, much higher than that reported for other *N*-donor containing aromatic heterocycles. (Table 1). However the CO_2/N_2 selectivity of PPN-101 half of that of the PPN-6 series, as high as 400 for PPN-6-CH_2DETA.[20] However the porosity and BET surface area is considerably higher than the 555 m^2/g of PPN-6-CH_2DETA. As previously mentioned this is due to the post-synthetic modifications of PPN-6 filling the pores and adding weight reducing from the base value of 4023 m^2/g.[63]

Table 1 summarizes all the aforementioned base-incorporated PPNs. The low production expense, considerable surface area, and large CO_2/N_2 selectivity indicated that PPN-101 a promising material for industrial CO_2 sequestration.

	TFM-1	**CTF-P6**	**Aza-CMP**	**BILP-1**	**PPN-101**	**PPN-6-CH_2DETA**
Incorporated Units	Triazine	Triazine	Pyrazine	Benzimidazole	Benzimidazole	Polyamine
Basicity (pKa)	<0.5	<0.5	0.65	5.532	5.532	$pK_{a,1}$>10
BET Surface Area (m^2/g)	738	1152	24 [a] /1227 [b]	1172	1096	555
CO_2 Uptake (273K, mg/g)	76.1	148.1	N/A	188	226.2	189
Selectivity of CO_2/N_2	29±2	16.1	N/A	~70	199	~400
PSM required	No	No	No	No	No	Yes
Ref	[67]	[68]	[69]	[71]	This Work	[20]

Table 1 Comparison of carbon dioxide uptake and sorption properties of representative PPNs

2.2.4 Adsorption of other gases of interest in PPN-101

In addition to the carbon dioxide uptake, PPN-101 was investigated for other gases of interest, specifically H_2 and CH_4 uptake. The low cost synthesis would make this PPN an attractive alternative to other materials studied for storage applications. The H_2 uptake at 77 K and 1.21 bar (906 mmHg) is 214.18 cm^3/g (1.91 wt %, Figure 8 (a)), this is similar BILP-1 (19 mg/g, 1.86 wt %)[71] and larger than other porous materials with similar surface areas.[75] However, this value is almost exactly what is expect according to Chahine's rule which states that 1 wt% of excess hydrogen adsorption is expected per 500 m^2/g of surface

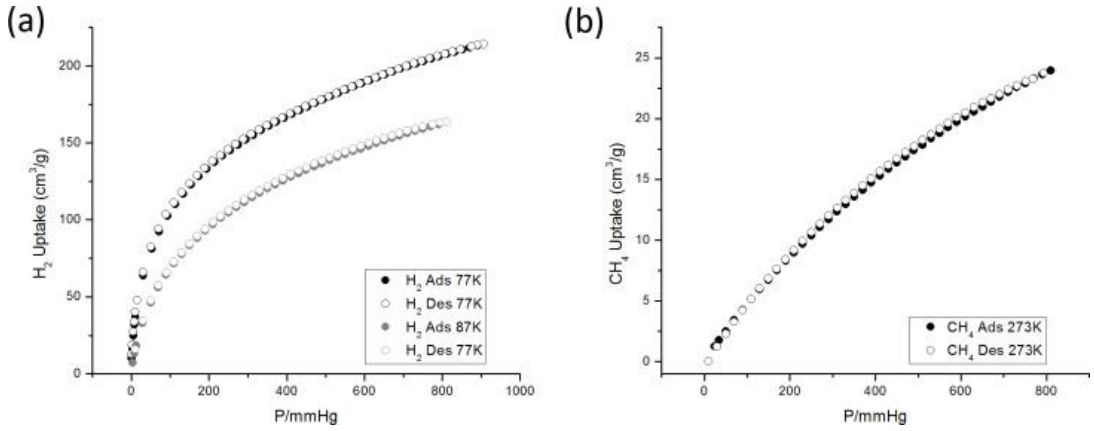

Figure 8 Hydrogen and methane isotherms for PPN-101[21]

area. Chahine's rule is formulated assuming hydrogen adsorption on graphite and fits well with the fused aromatic structure of the benzimidazole units in these materials. The methane uptake of 24 cm^3/g at 273 K (Figure 9 (b)) is respectable but not remarkable for this class of materials. In addition the low density of these materials means that they could never meet the volumetric needs in vehicular storage applications for either methane or

hydrogen.[1, 11, 20, 63]

2.3 Future Work

When this work was originally published PPN-101 stood out as a potential candidate for carbon due to its good performance and low production costs. The benzimidazole units provide a high selectivity for CO_2 compared to many other systems and provide a carbon dioxide fixing moiety directly into the structural backbone allowing for the pore volume to remain large. However in retrospect PPN-101 suffered from several issues that were not considered prior to the original publication. When also considering the synthesis of the silane monomer and the low temperatures required this becomes too costly given the performance of the material at room temperature since in a CCS system the temperature would likely be approximately 40 C. Further work on benzimidazole polymers has been conducted as sorbents[21, 71, 76-78] and as mixed membrane components[12, 79-80] as well as in simulated application environments.[23] Many of these have better performance than PPN-101 though they are more costly. If a cheaper route to benzimidazole PPNs can be found their use as sorbents may be found competitive, however, if not their inclusion in mixed matrix membranes where they contribute only a portion of the cost and the process may be more efficient could offer a better solution.

Additionally subsequent works from the Zhou group have produced materials that are both cost-effective and highly selective.[65] Another method previously researched but largely

eschewed due to the lower amine losses in tethered materials is loading a cost-effective material with free polyamines. This has been achieved in the PPN-150 series.[81] This PPN is based on a melamine-formaldehyde condensation polymer, originally published by Tan and coworkers[82] that has been loaded with DETA, a formulation developed in the Zhou group. While free amines generally escape a porous material over many cycles, by controlling cycling behavior cycling losses can be limited and uptakes between 10 and 20 wt% have been observed. However, when tests were performed at the 1 L sorbent scale control over amine losses was lost. When the material synthesis and breakthrough testing wash scaled to the lab scale (250 g) performance issues such as lowered porosity and amine leaching become obvious causing fowling of the equipment and low CO_2 uptake across cycling conditions. Further work in this area to tune the porosity of the material to better hold the amines may make this a competitive sorbent due to its cheap synthetic cost, both the paraformaldehyde and melamine starting materials can be obtained at a price two orders of magnitude cheaper than that for PPN-101, and high uptake potential.

2.4 Experimental

2.4.1 Materials and Instrumentation

The tetrakis(4-formylphenyl)silane was synthesized by a previously reported procedure with slight modification by Muwei Zhang.[74] Benzene-1,2,4,5-tetraamine tetrahydrochloride, *N*,*N'*-dimethylformamide (DMF), were purchased from VWR.

Infrared spectroscopy (FTIR) data were collected using a SHIMADZU IRAffinity-1 FTIR Spectrophotometer.

Powder X-ray diffraction (PXRD) was carried out with a BRUKER D8-Focus Bragg-Brentano X-ray Powder Diffractometer equipped with a Cu sealed tube ($\lambda = 1.54178$) at 40 kV and 40 mA. Elemental analysis (C, H, and N) were performed by Atlantic Microlab, Inc. (Norcross, Georgia). Thermogravimetric analyses (TGA) were performed on a SHIMADZU TGA-50 Thermogravimetric Analyzer with a heating rate of 5 °C min^{-1} under N_2. A Micrometritics ASAP 2020 Gas sorption analyzer was used to collect all isotherms. The various temperatures were achieved using a dewar flask and liquid nitrogen (77 K), liquid argon (87 K), dry ice/Acetone bath (195 K), ice bath (273 K), and tap water (296 K).

2.4.2 Synthesis

2.4.2.1. Synthesis of PPN-101

Synthesis of tetrakis(4-formylphenyl)silane

A 500 mL round bottom flask equipped with a condenser was pumped under vacuum and refilled with N_2 three times before the dry 4-bromobenzaldehyde dimethyl acetal (pre-dried by molecular sieves, 10.90 mL, 52.5 mmol) was added. Freshly distilled THF from a solvent still (300 mL) was carefully added to the flask through a cannula. The

solution was cooled to -78˚C by a dry ice/acetone bath. At this temperature, n-butyl lithium (20 mL, 2.5 M in hexane) was added dropwise slowly over a period of 1 hour. The reaction mixture was kept at -78˚C for an additional 2 hours before $SiCl_4$ (1.14 mL, 10 mmol) was added dropwise. The mixture was stirred at this temperature for an additional 2 hours before it was warmed up to room temperature and kept overnight. The reaction mixture was quenched with 2 M HCl (60 mL) and extracted with ethyl acetate (100 mL×3). The combined organic phase was washed with brine, dried over $MgSO_4$ and evaporated to give the oily intermediate acetal product $Si(4\text{-}C_6H_4CH(OEt)_2)$, which was hydrolyzed without purification. The oil was dissolved in 100 mL THF/HCl (*aq*) and the mixture was refluxed for 2 hours. The reaction mixture was quenched with enough $NaHCO_3$ till no more formation of CO_2 was observed and extracted with ethyl acetate (100 mL×3). The combined organic phase was washed with brine, dried over $MgSO_4$ and evaporated to give an off-white solid as the crude product. A recrystallization in EtOAc/Hexane afforded 3.24 g white crystalline powder as the final product (72.32%). ^{1}H NMR (300 MHz, DMSO-d_6): δ = 10.08 (s, 4H, CHO), 8.01 (d, 8H, Ph), 7.75 (d, 8H, Ph).

Synthesis of PPN-101

PPN-101 was synthesized by a similar synthetic route as BILP-1. [71] The aldehyde monomer tetrakis(4-formylphenyl)silane (134 mg, 0.3 mmol) was dissolved in anhydrous DMF, and under N_2 atmosphere, the other monomer 1,2,4,5-

tetrabenzeneamine tetrahydrochloride (176 mg, 0.6 mmol) dissolved in anhydrous DMF were added dropwise at -30 °C. An orange precipitate was formed very slowly in the solution. The reaction was kept cold until no more precipitate was formed and then allowed to warm to r. t. overnight. Then the reaction mixture was placed under an O_2 atmosphere and directly refluxes under O_2 for 2 days. (***Caution***: This step should be handled in an extremely cautious way to prevent any possible combustions or explosions. Protective shields should be used during the process of reaction). The polymer was centrifuged and washed with DMF then dried *in vacuo* to give a yellow/tan solid (119 mg) in 59.2% yield. (IR: 725 (s), 829 (s), 1018 (m), 1085 (m), 1294 (m), 1249 (m), 1610 (s), 2312 (w, br), 3616 (w, br). Calculated for $C_{40}H_{28}N_8Si$: C, 74.05%; H, 4.35%; N, 17.27%; Si, 4.33%. Found: C, 74.50%; H, 4.13%; N, 16.93%; Si, 4.07%.)

2.4.3 Characterization of PPN-101

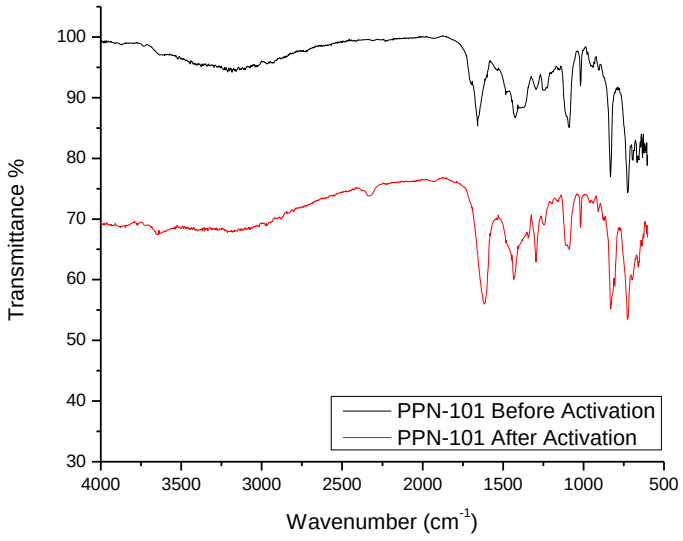

Figure 9 FTIR spectrum of PPN-101 before and after activation[21]

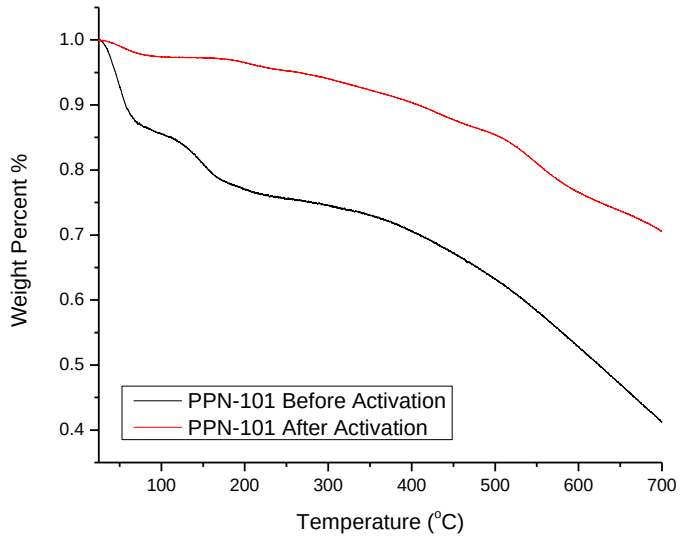

Figure 10 TGA of PPN-101 before (black) and after (red) activation

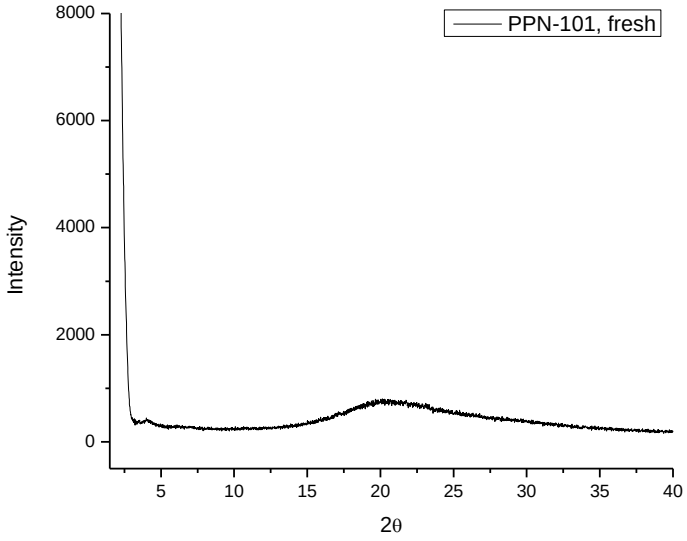

Figure 11 The PXRD of the as synthesized sample of PPN-101[21]

2.4.4 Activation Procedures and Additional Gas Sorption Isotherms for PPN-101

The fresh polymer sample was washed with DMF three times for 3 days, methanol twice for 2 days, and acetone twice for 2 days. After activation at 80 ºC for 8 h, it had resulted in a fluffy bright yellowish polymer with the BET surface area 996 m^2/g and Langmuir surface area 1613 m^2/g. After activation at 120 ºC for 12 h, the BET surface area was improved to 1096 m^2/g and Langmuir surface area 1799 m^2/g. This is probably due to the incomplete removal of the H_2O molecule residing at the Lewis base sites at lower temperatures. [71] Figure S4 shows the N_2 and Ar adsorption data of PPN-101 activated at both 80 ºC and 120 ºC. A significant increase of the both N_2 and Ar uptake was observed when the sample was activated at an elevated temperature. Further increase of activation temperature does not result in a significant improvement of surface area or a significant decrease of the weight of the sample.

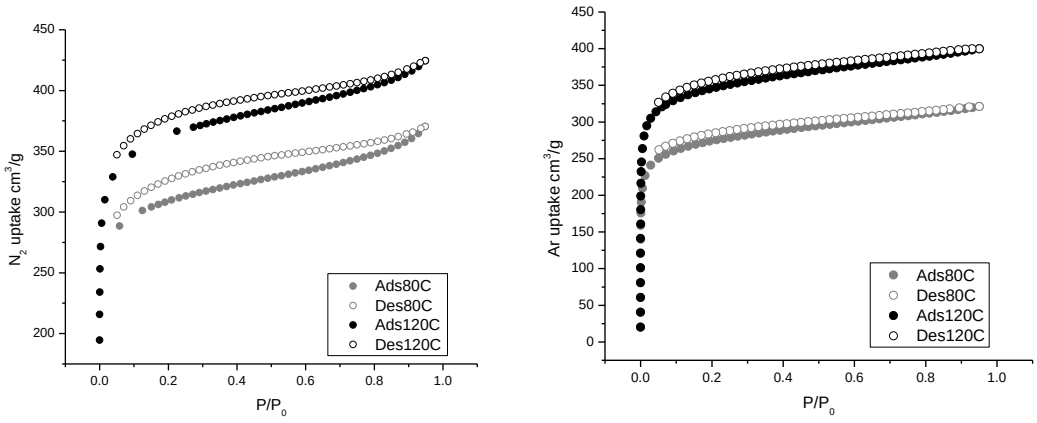

Figure 12 (a) The N_2 uptake isotherm of PPN-101 samples activated at 80 and 120 ºC. (b) The Ar uptake isotherm of samples activated at 80 and 120 ºC[21]

The following gas adsorption isotherm (Figure 13) was measured from the fully activated sample (120 ºC, 12h).

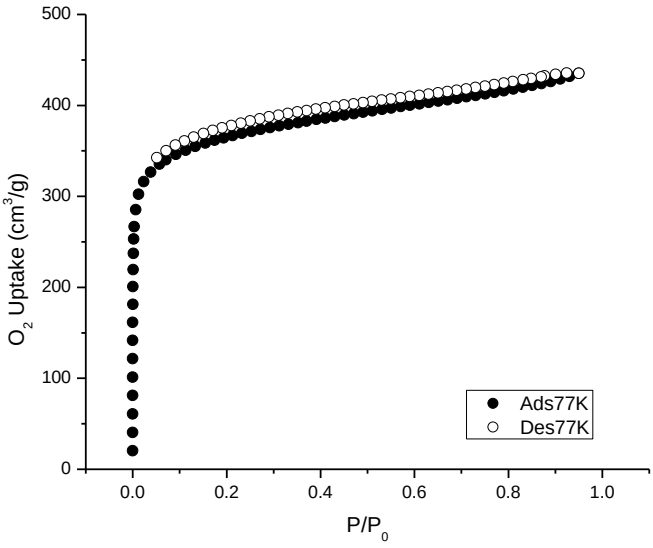

Figure 13 The O_2 uptake isotherm of PPN-101 at 77K and 1 bar[21]

2.4.5 Calculation of CO_2/N_2 Selectivity

The selectivity of CO_2/N_2 of PPN-101 in flue gas conditions was evaluated from the composition of flue gas where the partial pressure for CO_2 is 0.15 bar and N_2 is 0.85 bar. [10] The uptake of CO_2 at 0.15 bar and N_2 at 0.85 bar were estimated by linear interpolation, and the selectivity is calculated by using Eq. 2.

$$\boldsymbol{Selectivity} = \frac{\boldsymbol{Q_{CO_2}/Q_{N_2}}}{\boldsymbol{P_{CO_2}/P_{N_2}}} \qquad \textbf{Eq. 2}$$

In Eq. 2, Q indicates the quantity of the absorbents, while P indicates the partial pressure. The calculated CO_2/N_2 selectivity of BIPPN-1 in flue gas at 273K was calculated as 199.

CHAPTER III

GAS ADSORPTION WITHIN POROUS MATERIALS DERIVED FROM METAL-ORGANIC POLYHEDRA WITH CHROMIUM(II)-TETRACARBOXYLATE PADDLE WHEEL NODES*

3.1 Introduction

The scope of porous coordination materials extends from zero to three dimensional coordination structures namely metal-organic polyhedra (MOPs) and metal-organic frameworks (MOFs).[9, 57, 83-84] The regular order of MOFs in 3D space gives them structural rigidity and access to permanent porosity. [85] MOPs are however defined by their discrete nature and structurally defined pore space.[8, 84, 86-89] Several MOP based materials have been reported with measured porosity.[41, 46, 48-50, 90-94] While discrete MOP structures have a pore volume defined by the cage structure until recently materials consisting only of coordination cages supported without bridging through metal coordination have rarely demonstrated significant porosity. This is due to a number of factors including both the stability of the discrete cages as well as the extended structure of the material with respect to activation conditions. This has typically resulted in materials with a much lower porosity than would be expected from theory.[95-96] However,

---

* Part of the data in this chapter is reprinted and adapted with permission from Park, J.; Perry, Z.; Chen, Y. P.; Bae, J.; Zhou, H. C., Chromium(II) Metal-Organic Polyhedra as Highly Porous Materials. *ACS Appl Mater Interfaces* **2017,** *9* (33), 28064-28068. Copyright American Chemical Society 2017.

some of the previous successful examples relied on crystal engineering principles to improve the rigidity and ultimately the stability of such materials. To that end two separate methodologies had been developed and applied to achieve observable porosity. The first developed method utilizes known mesoporous silicas and metal-organic

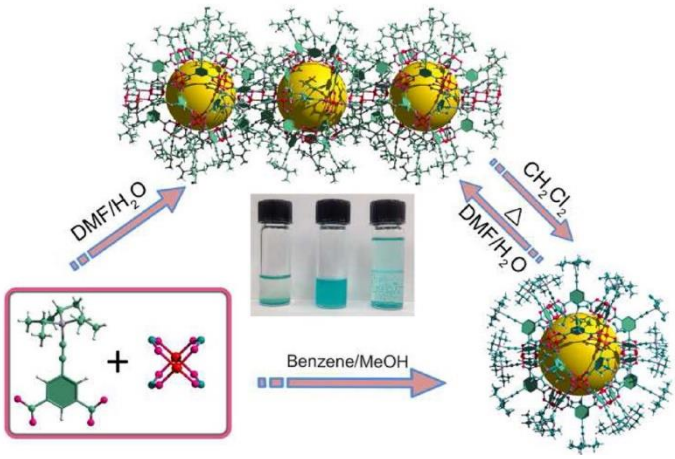

Figure 14 Solvent polarity controlled interconversion of copper TEI MOP from discrete cage (right) to infinite chain through dimetal paddle wheel self-association through bridging of carboxylates(top).[41]

frameworks which have cavities large enough to encapsulate the discrete MOPs. By dispersing the cages within these pores at relatively low coverage their discrete nature is preserved and changes in the porosity can be measured. This was confirmed by observation of behaviors within the composite materials that derive from the specific features of the MOPs such as windows and cavity size.[97-99] The second method uses intermolecular interactions to create interdigited MOPs creating chain-like structures through formation of coordination bonds that bridge the individual cage species(Figure 14).[41] In this case reported by the Zhou lab, solvent polarity was used to drive a single-

crystal to single-crystal transformation. The bulky and hydrophobic triisopropylsilylethynyl directs the di-copper paddlewheel units to associate similarly to that of anhydrous chromium acetate.

Many record-breaking materials and some of the top-performing materials for gas storage applications are based on dimetal paddle wheel units, almost exclusively copper(II), and often bridged by isophthalic acid derived ligands.[100-101] While these paddlewheels typically exist as discrete $M_2(RCOO^-)_4L_2$ groups chromium(II) examples are known to self-associate if no advantageous ligand is available.[102 103] The high axial ligand affinity coupled with the stability afforded by the multiply bonded centers stabilizes the paddlewheel structure. The "locking" of dimetal paddlewheels due to orbital orientations required for metal-metal bonding is well studied.[104-105]

In particular a molybdenum paddle wheel based core-shell structure, published by the Zhou lab, demonstrates the ability for a multiply bonded metal node to absorb stress induced by the structure (Figure 15).[35] In this unique core-shell structure two individual coordination structures exist with one nested within the other. This behavior arises from the flexibility of the ligand and as well as the fact that the void space within the outer shell matches both the symmetry and functionality with that of the core species. Upon exchange at sites I and II (Figure 15c) from molybdenum to copper the paddlewheel twists by an additional ~15° decreasing the distance between the hydrogen bonding sites at the amides (Figure 16). This core-shell structure cannot be obtained directly from

copper salts. This indicates that the presence of a metal-metal multiple bond enables observation of a structure that otherwise could not be resolved utilizing an analogous secondary-building unit without that bonding. Additionally the resulting twist shows that the bond is absorbing some of the strain within the system that is relaxed when the non-bonding copper is substituted.

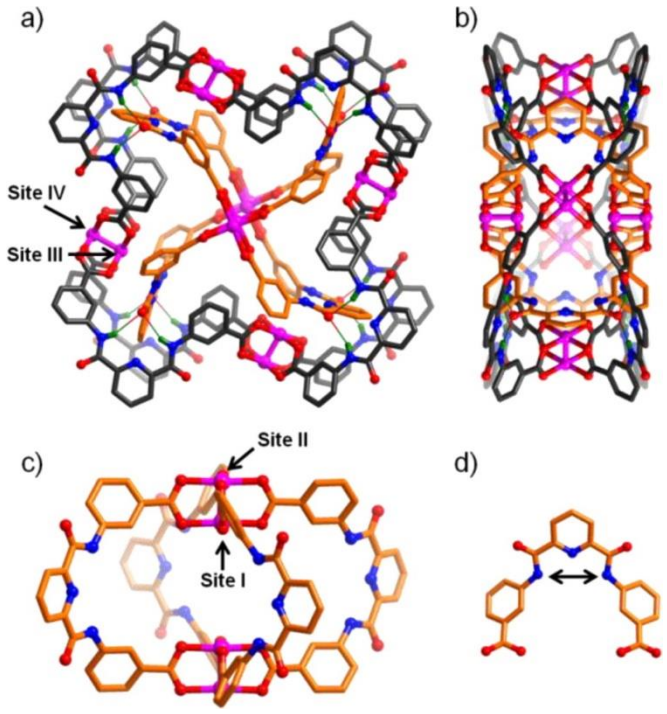

Figure 15 Molybdenum core-shell MOP from a) Top and b) side. c) Core lantern shaped cage consisting of two M_2 paddlewheels and and four ligands in the orientation shown in d). Sites I and II are ~100% Cu after exchange.[35]

When the chromium MOP work was first published it was hypothesized that such a self-association mechanism could explain the observation of porosity in Cr(II) paddlewheel based cages that is not seen in isostructural Cu(II) systems.[29-30, 106-110] Based on further

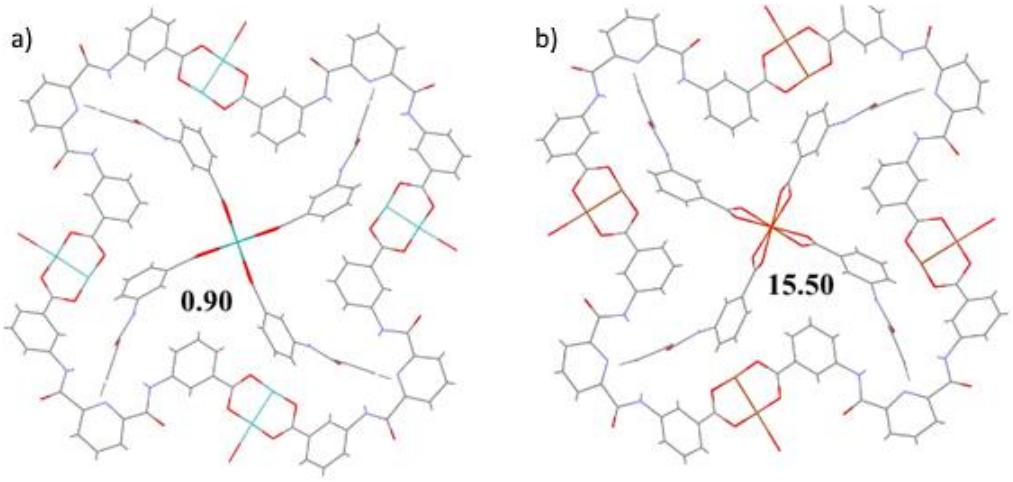

Figure 16 a) Mo(II) core-shell MOP and torsion angle of Mo paddle wheel b) Cu(II) core and 3:1 Mo:Cu shell after substitution[35]

considerations this mechanism is no longer thought to accurately reflect the entirety of the system as discussed in Chapter IV of this dissertation. Through functionalization of the 5-position in isophthalic acid porosity was achieved in each of the systems through thermal activation. The resulting chromium(II) based systems have BET surface areas as high as 1000 m^2/g higher than many other such systems. These were also the first Cr(II)-based MOPs reported in the literature[47] and although not the first porous Cr(II)-based compounds, two previous Cr(II) containing MOFs have been published by the Long group,[93, 111] they are also the first to be able to be solved using single crystal diffraction

methods. Several other Cr(II) based MOP materials have been published by the Bloch group since that original publication.[49-50, 93]

3.2 Results and Discussion

Four different isophthalic acid derived ligands were selected for the porosity study based on previous experience and published works (Figure 17).[38-39, 41, 112-113]

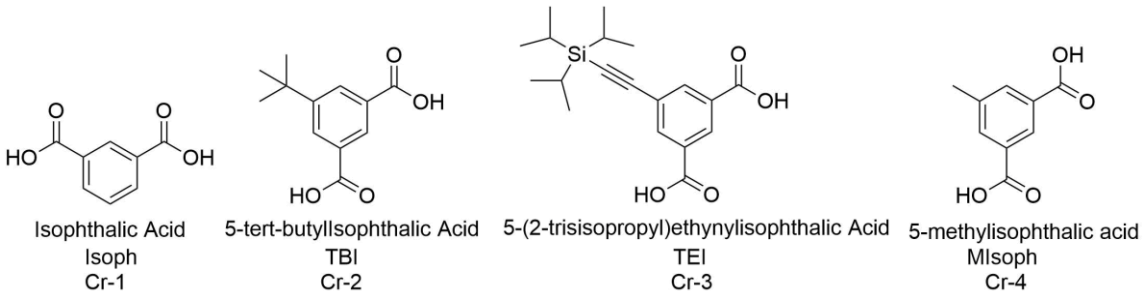

Figure 17 Isophthalate and 5- substituted isophthalate ligands used to synthesize porous chromium MOPs, Cr-1-4

The cages obtained with these ligands have the same basic structure as those reported by Yaghi and Zhou for dimetal paddle wheels with copper, molybdenum, and ruthenium nodes.[113-115] The structure of these $M_2(_{12})$ L_{24} MOPs is cuboctohedral in nature consisting of M_2 paddle-wheel vertices, ligands along the edges, and windows serving as the triangular and square faces (Figure 18).[29] The Cr-Cr bond distance within the MOPs of 2.36 – 2.39 Å matches well with that reported value of 2.36 Å for chromium acetate and is significantly longer than that seen in carboxylate bridged di-chromium paddlewheels with no axial coordination of 1.97 Å.[103] This Cr-Cr distance is

predominantly controlled by the presence of the axial ligands with gas-phase chromium(II) acetate having a distance of 1.96 Å.[116] Porosity was first successfully observed in MOPs with three ligands with the TEI ligand giving rise to two distinct packing motifs all with the same cuboctahedral structure for the MOPs.

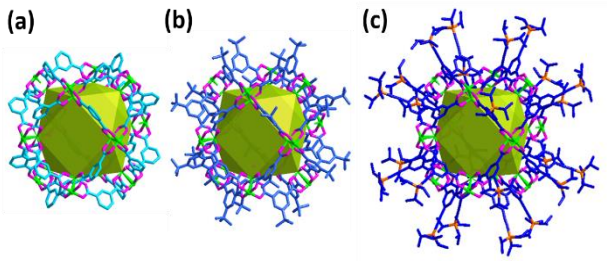

Figure 18 Chromium(II) cuboctahedral cages obtained from (a) isophthalic acid (b) 5-tert-butylisophthalic acid, and (c) the TEI ligand[47]

To achieve porosity, a number of factors had to be considered. First was the solvent exchange step, this was chosen to be the same as the synthesis solvent to ensure that a) the cage had a low solubility and b) any remaining acetate or ligand would be removed. Then a second solvent was needed to replace the non-volatile amide based solvents DMF, DMA, and DEF (*N*,*N*-dimethylformamide, *N*,*N*-dimethylacetamide, *N*,*N*-diethylformamide, respectively) with one that would not induce pore collapse upon activation. Since these compounds were being handled in a glovebox, non-protic solvents were considered and with the hindsight of the changes such materials may undergo in polar or coordinating solvents as observed in the Cu-TEI MOP previously published by the group such solvents were also excluded.[41] For these reasons toluene

was chosen for Cr-1 and Cr-2 while hexane was used for both topologies of Cr-3 as this cage was found to be soluble in toluene. The TEI ligand enabled solubility of the cage in toluene, diethyl ether, and benzene, among others non-polar solvents.[41, 117] As the goal in this project was to study the effects of replacing the typical copper for chromium paddlewheels maintaining the discrete nature of the cages was considered a priority.

Upon activation, these MOPs exhibited significant color changes from dark purple for the as synthesized materials to a light purple after solvent exchange and initial drying and finally yielding a yellow/tan colored product. The as synthesized material fresh from the mother liquor can be handled briefly in air and placed under oil for mounting on a crystal loop and similarly may be used to collect PXRD patterns but will oxidize within several minutes in air. After exchange with toluene or hexane the materials decompose quickly as the more volatile solvents evaporate from the pores. After activation extreme care was needed and many samples were lost in developing methodologies for acquiring gas adsorption data. Thus the data reported was obtained from strict handling procedures and only those samples that showed no visible signs of oxidation, present as a greening or darkening of the activated solid, were used for gas adsorption measurements. The N_2 uptakes and porosity determinations for these compounds are given in Table 1. These materials showed significantly higher uptake than the related isostructural copper and molybdenum MOPs after thermal activation.

Table 2 N_2 adsorption values, surface areas, and porosity values for chromium(II) MOPs and Cu-TEI MOP material

	Cr-1	Cr-2	Cr-3_{rhom}	Cr-t_{tet}	Cr-4	Cu-TEI
BET	833.4	1084	579.8	708.5	574.4	739
Lang. SA	1161	1496	618	1020	796.5	843
Pore Vol.	0.45	0.60	0.20	0.35	0.28	0.29
Reference	[47] ([49])	[47]	[47]	[47]	This Work	[41]

The calculated BET and Langmuir surface areas of the Cr-MOPs were determined utilizing the Brunauer–Emmett–Teller theory selecting at least five points that provided the best linear fit between .05 and .30 p/p^0 as is appropriate for microporous materials.[52] The best performance was observed in Cr-2 with a BET SA of 1084 m^2/g and a Langmuir SA of 1496 m^2/g. At the time of publication this was the highest reported value for an unsupported MOP with paddlewheel nodes, however, shortly after Bloch and coworkers published the same MOP with a slightly higher value of 1135 m^2/g.[49] This is in the range of many well-known MOF structures. This exceptional porosity indicates that the pore volume within the material after activation is accessible. The pore-size distribution indicates a major pore at approximately 15 Å which correlates to the pore width within the cage of approximately 16 Å from one metal center to another across the cage. Previous to this work the only porous metal-organic materials containing Cr^{2+} ions were Cr(BTC) a structural analogue of the well-known HKUST-1 and Cr-BTT both reported by the Long group.[118-120] A large portion of the MOF

literature has focused on copper paddlewheel MOFs and many records such as surface area and maximum hydrogen and methane uptakes have been held by such MOFs over the past two decades.[1, 75] However, the distinct difference between molecular cages and those extended structures is that the regular packing through the structure is maintained by non-covalent intramolecular interactions rather than molecular or dative bonding. That means that when the paddlewheels are desolvated at high-temperatures and high vacuum the rigidity of the extended structure is maintained. However, within MOPs the structure is more tenuously balanced and when desolvation occurs a significant strain on the metal nodes may cause them to fall apart. As is seen in the works by Long the isostructural chromium and copper MOFs have similar levels of performance and surface area, though the chromium materials tend to perform below what might be

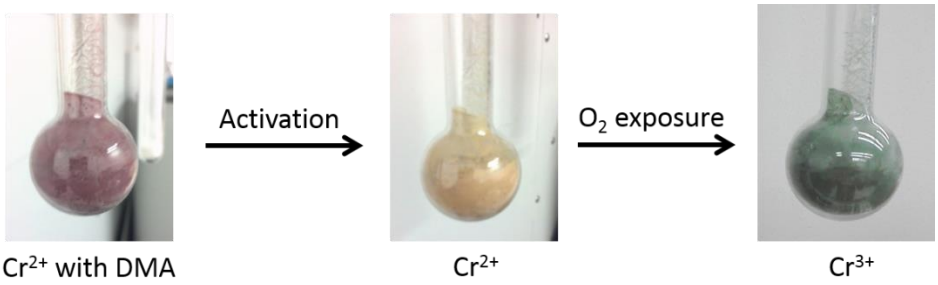

Figure 19 Color change from dried, activated, and oxidized Cr-2[47]

expected when mass is considered. This may be in part due to the synthetic methods applied and the nature of MOFs which often yield microcrystalline powders that may contain defects unlike the MOP syntheses presented here which can yield large single crystals.

As a performance reference, isostructural copper MOP crystals (Cu-TBI) were synthesized and subjected to the same activation scheme as the isolated chromium cages. The copper cage shows gradual improvements in N_2 uptake after activation at temperatures from 80 °C to °160 C, however, at °200 C the pores completely collapse and porosity is no longer observed (Figure 20a). Cr-2 (Figure 20(b)) in contrast shows no significant uptake until activated at 200 °C wherein it displays a type-1 isotherm and significant hysteresis. It is reasonable given these results to attribute the greater stability afforded to the dichromium paddle wheels to the metal-metal which enables maintenance of the cage structure when the axial ligands are removed.

Since the cages have internal surface areas identical to one another, the difference being that of the functional groups at the 5-position, a non-traditional method was devised to

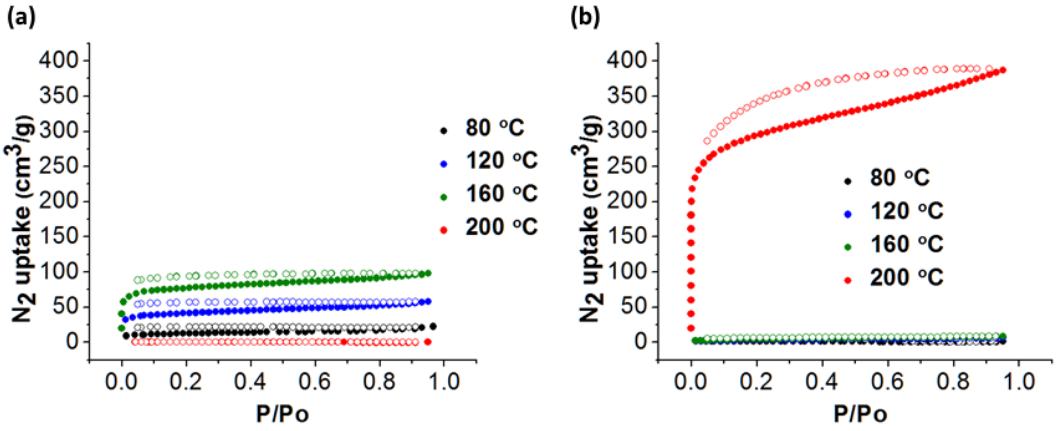

Figure 20 Activation effects on N_2 uptake at 77 K for a) Cu-TBI and b) Cr-2 activated at each temperature for 10 to 12 hours at a maximum vacuum of 8 µBar[47]

compare the relative performance of these systems. Rather than a traditional gravimetric surface area represented as m^2/g the surface area for each system was normalized per mole of cage which is represented as a value of km^2/mol of cage. In doing so the surface areas can be evaluated based on how much of each cage is accessible on average which would normally be occluded by the presence of bulky functional groups.

Table 3 Molar masses, BET gravimetric surface area and calculated BET molar surface area per cage pore

	Cr-1	Cr-2	Cr-3_{rhom}	Cr-3_{tet}	Cu-TEI	Mo-TBI
MM Cage	5207.0	6552.4	9530.1	9530.1	9807.3	7607.1
BET SA	833	1040	580	709	739	437
Molar BET km^2/mol	4.34	6.84	5.53	6.75	7.25	3.32
Lang. SA	1161	1406	618.0	1020	843	504

The expected trend based on the relative size of the functional groups would be Cr-1<Cr-2<Cr-3 as the large functional groups should increase accessible surface area outside of the cages as well as provide additional surface area themselves. As expected Cr-1 is indeed the lowest but as with the total surface area Cr-2 is higher than Cr-3. The difference between these values is significantly lower than that of the total surface area and the value for Cr-3_{Rho} is lower than that of Cr-3_{Tet}. The significantly lower

performance of Cr-1 is attributed to the lack of strong interactions or bulky functional groups keeping the cages from aggregating. The lower than expected performance of Cr-3 both tetrahedral and rhombohedral crystals was attributed to the large voids between the space leading to aggregation and reducing pore-accessibility in much the same way, however upon inspection of a normalized factor for gas adsorption based on a per cage basis Cr-3_{tet} performs almost as well as Cr-2.

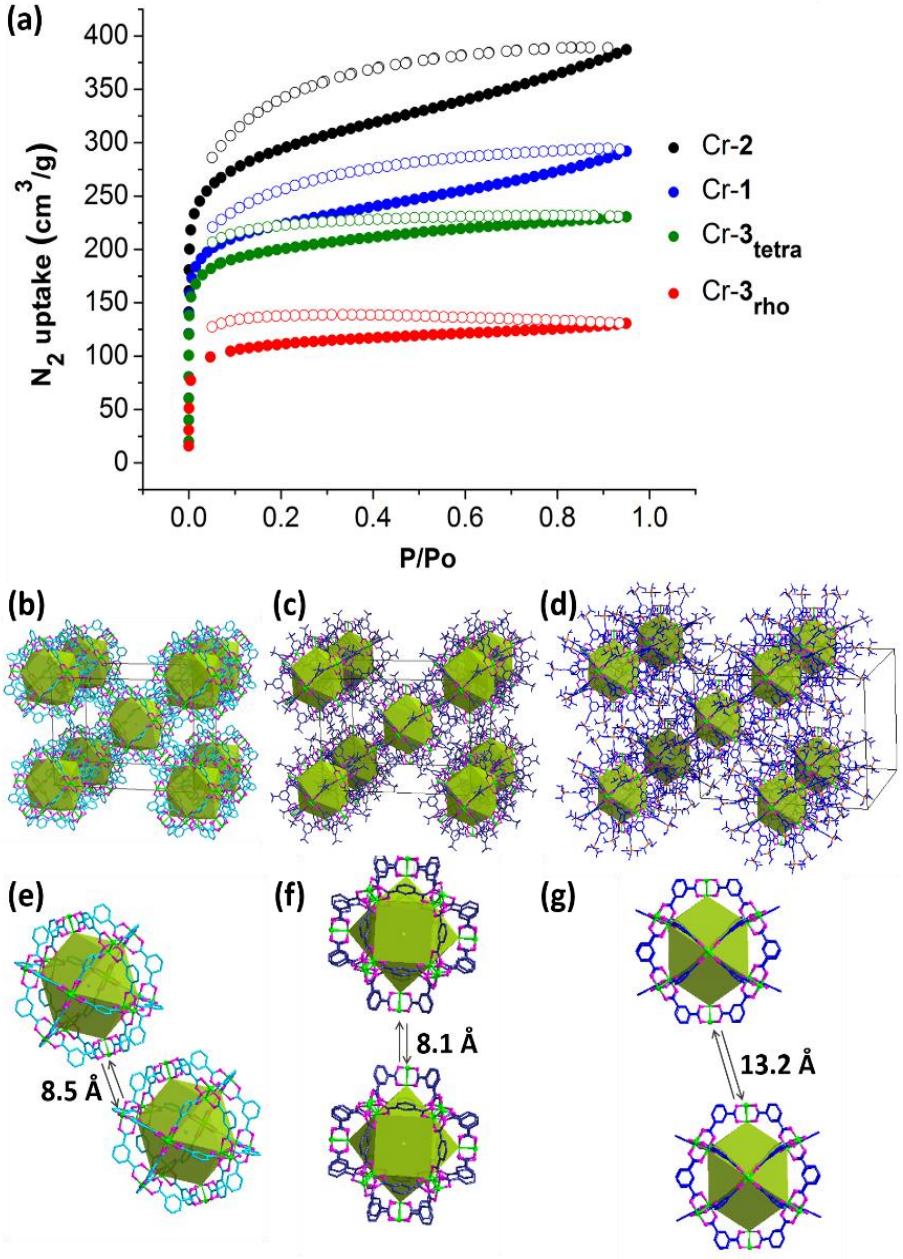

Figure 21 N2 adsorption (a), packing of chromium MOPs and the closest intramolecular paddlewheel distances for each MOP: Cr-1(b,e), Cr-2(c,f), and Cr-3$_{tet}$(d,g) functional groups and hydrogens removed for clarity.[47]

The N_2 77 K sorption isotherms show inflection of the adsorption portion and hysteresis in the desorption portions of the isotherms.[121] The inflection can be attributed to formation of larger mesopores as seen in the sloping nature of the isotherms after the initial microporous region, as compared to the plateau like nature of true type-1 isotherms.[95, 122-123] Additionally the small pore windows and aggregation of the cages produces bottle neck effects in the desorption phase. The gas molecules thus cannot exit the pores at the same pressures they entered due to capillary effects giving rise to the observed hysteresis.

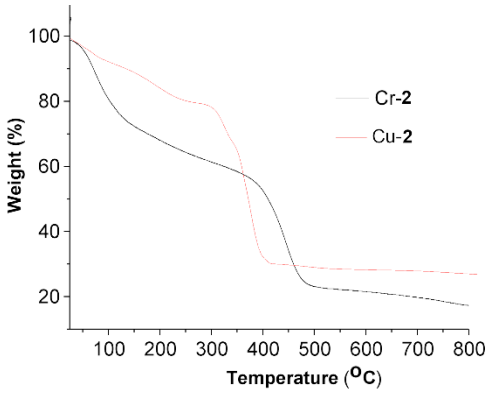

Figure 22 Thermogravimetric analysis curves for Cr-2 (black) and Cu-2 (red)

It is proposed that the difference in porosity under the activation regimes seen in the copper and chromium MOPs arises from the fundamental differences between the paddlewheel complexes. As seen in their respective TGA curves (Figure 22). While the TGA curves cannot give information regarding the structural collapse the approximately

100 °C difference in the onset of the steep drop in mass, attributed to loss of coordinated solvents, indicates that the copper desolvates at a lower temperature than the chromium species. This matches the observed activation data in Figure 20. This explains why a significantly higher temperature is required to activate the chromium based materials as the elevated temperature is required to successfully desolvate the chromium cages. Further the presence of the metal-metal bond is proposed to facilitate the stability of the individual cages as compared to the copper which lacks the additional support. The copper paddle wheels have no direct bonding interactions even though each atom contains an unpaired electron. Once desolvated it is proposed that the copper acetate moieties rearrange due to the stress imposed by the aggregated solid, similar to the twist

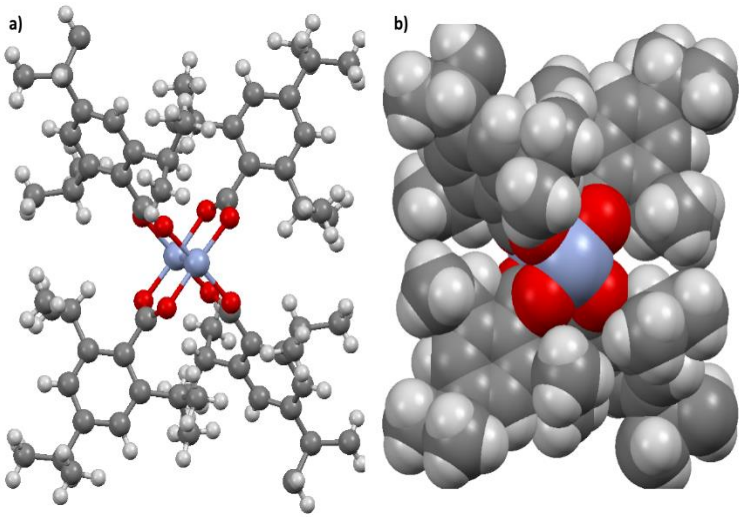

Figure 23 The first ultra-short Cr-Cr quadruple bond demonstrated in a carboxylate bridged paddlwheel a) ball and stick model for clarity and b) spacefilling model showing steric bulk that prevents self-association of complexes through carboxylate bridging.

observed in the core-shell system. Once such a distortion is severe enough the paddle wheel and thus the cage decompose. The chromium system however can maintain the paddlewheel shape in the absence of such an axial ligand, as shown by Cotton and coworkers (Figure 23), when an axial ligand is not present and steric bulk prevents aggregation of the paddlewheels through carboxylate bridging. It has been suggested that such a bridging mechanism is a possible way in which the chromium cages are stabilized, much as the copper(II) TEI system was, but this is unlikely as while such structural rearrangements were single-crystal to single-crystal they were still solvent supported which is not the case in the chromium cages under discussion here. Though some such self-association may occur in these systems it is unlikely to occur to the degree of that previous publication. The stability of these systems must then be attributed to the reinforcement of the structure through the Cr-Cr quadruple bond and any intermolecular interactions between the cages. The intermolecular interactions driving the formation of these structures is discussed in Chapter 4.

The storage of methane and hydrogen was thought to be a potential use for these cuboctahedral cages as they contain similar structural features to many of the copper paddle wheel based MOFs[1, 7, 58] that have high uptakes such as HKUST-1,[124,] NU-111,

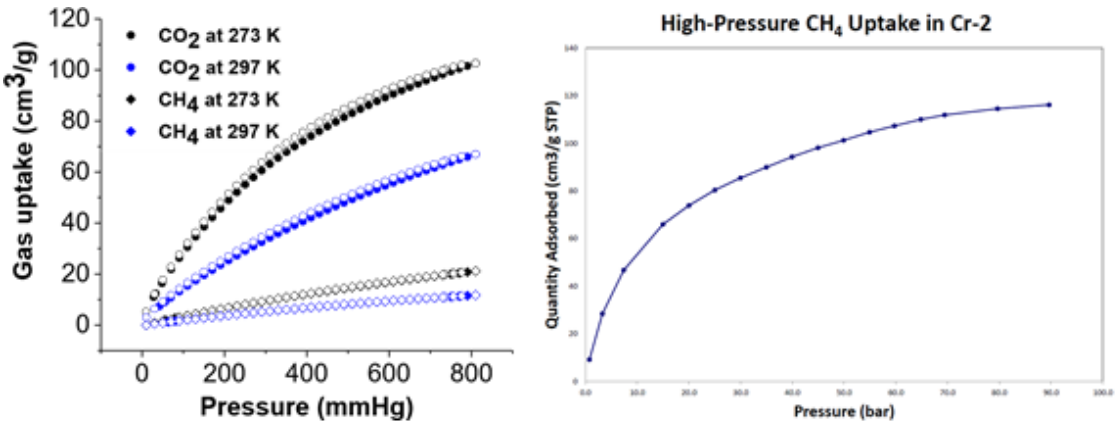

Figure 24 Carbon dioxide and methane uptake at 273 and 295 K (left) and high-pressure methane gravimetric excess uptake (right)[47]

[125] and PCN-14.[126] These MOFs are all constructed from copper paddlewheels and what can be considered isophthalic acid derivatives and contain trigonal windows of the same size as in the cuboctahedral MOPs. These windows have been identified as the primary binding site for methane in such systems rather than the open metal sites as previously thought.[7, 127-128] The room temperature CH_4 uptake was not significantly high, 15 cm^3/g, and the high-pressure gravimetric uptake maxes out at 120 cm^3/g at 90 Bar, far below the DOE target.[7] Bloch and co-workers have reported a Cr(II) coordination cage based on a carbazole ligand with measured uptake values of 194 cm^3/g at 65 Bar.

The potential for non-axially coordinated chromium paddlewheels to demonstrate reversible O_2 adsorption was of interest to both our work and others. The two chromium(II) based metal-organic frameworks published by the Long group showed some reversibility for oxygen and it was hoped that these molecular species might behave similarly.[93, 129] Cr-**2** demonstrates irreversible O_2 chemisorption at 295 K of 34 cm^3/g at 295 K (Figure 25x(a)).[119] This correlates to approximately one molecule of O_2 per paddwheel unit. This behavior was also observed in the material based on the same chromium cage by Bloch.[49] Work by Kitigawa on similar rhodium cages and CO binding showed a similar value of approximately one gas molecule per paddlewheel which is attributed to only the inside of the cages being accessible. At lower temperatures the adsorption can be considered semi-reversible, however in all cases the materials degrade upon cycling. Under purely physisorptive conditions N_2 and O_2 typically have similar uptake values, due to similar kinetic diameters and quadrupole moments indicating that the increased selectivity of O_2 is indeed derived from the presence of the divalent chromium centers.[130]

The Cr-2 material was then checked for stability following oxidation to see if the oxidized material had been templated by the original structure. Compared to unoxidized material, the oxidized material (Cr-**2**') demonstrated decreased H_2 uptake at 77 K, going from 149 cm^3/g to 71 cm^3/g. This is essentially the same as that of the activated copper analog, 70 cm^3/g. Importantly this indicates that upon oxidation the chromium material begins to behave very similarly to the copper based material which is known to have

collapsed during the activation process. This points again to the importance of the Cr-Cr bond in achieving porosity in these systems.

In contrast, HKUST-1, one of the most studied and successful MOFs in terms of impact and documented performance, is constructed from copper(II) paddlewheels and 1,3,5-

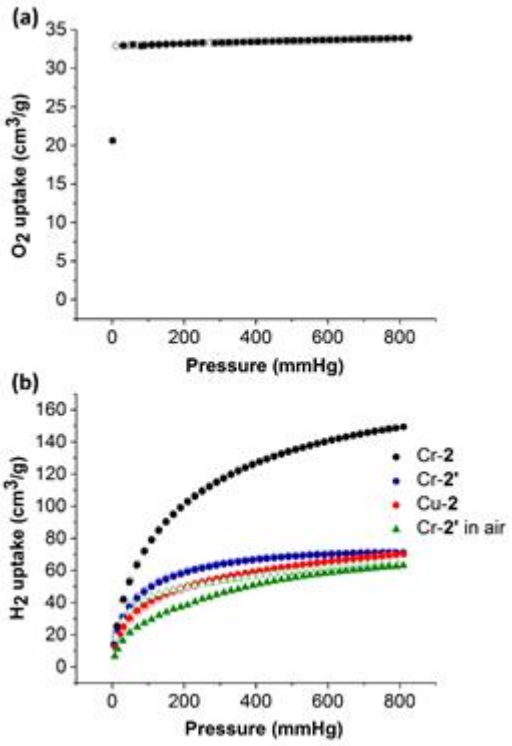

Figure 25 Oxygen uptake for Cr-2 at RT and the effect of O_2 exposure on Cr-2 H_2 uptake[47]

benzene tricarboxylic acid.[7, 124, 131-132] The stability of HKUST-1 under typical single-component gas sorption systems, that is not in the presence of water, is well known.[133] However the copper MOPs constructed from isophthalate ligands show no appreciable

gas uptake except in situations where they are dispersed or where strong intercage interactions have been formed.[95, 109, 124] Extension of the chromium MOPs via briding ligands between the paddle wheels has also been demonstrated to show increased gas uptake as compared to the pure cages.[94] The stronger bonds in these MOP-MOF materials stabilize them and prevent shifting in the structure that might cause collapse. This explains the similarities between the chromium and copper species after the oxidation events. While the copper MOP collapses during the activation procedure the chromium MOP maintains a level of porosity due to its metal-metal bond. However, once the paddlewheel is oxidized this bonding becomes weak and the structure can collapse in the same way as the copper system. This also explains the lack of reversibility in the O_2 adsorption as compared to the chromium(II) based MOFs. At higher temperatures the ligation of oxygen and subsequent oxidation of the chromium causes the weakening of the metal-metal bond. Without the support of the intermetallic bonding the stresses within the material caused by aggregation induce structural collapse. In the MOFs the extended network of coordination bonds maintains rigidity even in the absence of this bonding, as seen in HKUST-1 for copper, thusly preventing the immediate collapse of the structure. The higher oxygen uptake at lower temperatures can be associated with the system not having enough energy to drive the oxidation forward similar to that seen in porphyrin systems wherein the lack of an axial ligand prevents permanent oxidation of a divalent iron center by molecular oxygen.[134] There needs to be further work to identify the details of this phenomena but based on the

evidence collected and analyzed here and as well as that by the Bloch this mechanism seems likely. However further work will be needed to confirm these details.

3.3 Future Work

3.3.1 Expansion of scope in porous metal-organic polyhedra topologies

While the work in this dissertation focuses on cuboctahedral cages constructed from dichromium paddle wheels and substituted isophthalate ligands there exists a larger range of such paddle wheel based cage structures (Figure 26) that also have the potential for porosity. This range of cages have pore windows and volumes of varying sizes and since they are topologically defined by the angle of the bridging ligand extension of the ligand results in larger windows and pore sizes.[17, 32] Such cages have been demonstrated for both molybdenum,[39] and ruthenium[135] for the octahedral cage (Figure 26c). Thus far only the cubic $M_2(_6)L_{12}$ has been synthesized, by the Bloch group,[50] with Cr(II) and it shows remarkably high methane uptake for a molecular cage. A systematic study of these other cages' porosity through functional group control would provide a method of developing a wide variety of new materials for gas sorption. The cubic cage provides perhaps the best option for an initial study in this direction through functionalization of nitrogen in the carbazole ligand. Control of the arrangement of the cages and the interactions between them, discussed further in Chapter IV, may allow them to approach that of MOFs having the same size and shape pores seen in these cages.[50] However for

most of this work to occur a better understanding of what drives the extended structures of these cages to arrange in the way observed by various groups depending on synthesis

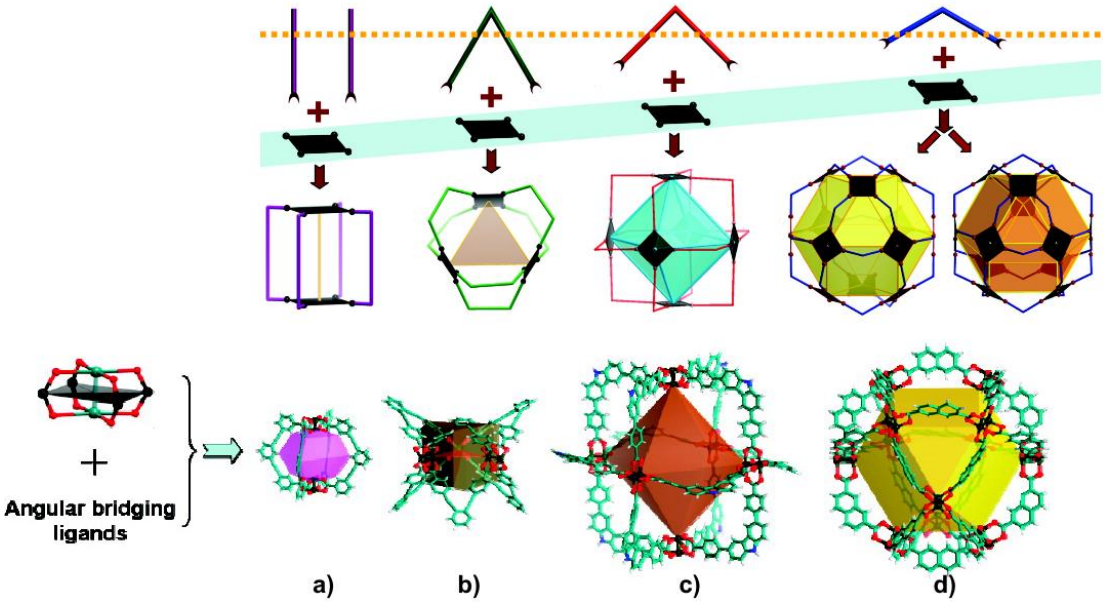

Figure 26 Bridging-ligand angle driven design of molybdenum paddle wheel MOPs resulting from the angle between carboxylic acids (top) to give cages a) 0° b) 60° c) 90° d) 120° (cuboctahedra) [39]

conditions. Chapter IV discusses the structural effects of ligand and solvents on the packing structures of these cuboctahedral cages and this can be extrapolated to the other shapes if a wider variety of them is synthesized and analyzed.

3.4 Experimental

3.4.1 Materials and Instrumentation

3.4.1.1 Instrumentation

^{1}H nuclear magnetic resonance (NMR) data to analyse the synthesized ligand was recorded on a Mercury 300 spectrometer at the Center for Chemical Characterization and Analysis (CCCA). FT-IR spectra was obtained in an IRAffinity-1 instrument. The TGA data was recorded by the use of a TGA-50 (SHIMADZU) thermogravimetric analyzer and Auto Q500 (TA Instruments) with a heating rate of 5 °C min^{-1} under 25 mL/min N_2 flow. A BRUKER D8-Focus Bragg-Brentano X-ray Powder diffractometer and Empyrean (Panalytical) equipped with a Cu sealed tube (λ = 1.54178 Å) was used to record the powder X-ray diffraction patterns (PXRD) of the MOPs at a scan rate of 0.5 s deg^{-1}. Gas adsorption isotherms were obtained by the use of Micromeritics' ASAP 2020 with the extra-pure quality gases.

3.4.1.2 Chemicals

Materials were used as received unless otherwise noted. Copper acetate monohydrate ($Cu_2(OAc)_4 \cdot 2H_2O$), chromium chloride hexahydrates ($CrCl_3 \bullet 6H_2O$), isophthalic acid, 5-tertbutylisophthalic acid were purchased from Alfa Aesar Chemicals. *N*,*N*-

dimethylacetamide (DMAc), *N*,*N*-dimethylformamide (DMF), and *N*,*N*-diethylformamide were obtained from Acros organic, Macron fine chemicals^{tm}, and TCI, respectively. Sulfuric acid was purchased from EMD. 99.9% Zinc Powder and Sodium acetate was purchased from Sigma-Aldrich, and ethanol from Koptec.

3.4.2 Syntheses

3.4.2.1 Triisopropylsilyl ethynyl isophthalic acid (H2TEI)

H_2TEI was synthesized as reported previously.[41]

3.4.2.2 $Cr_2(OAc)_4$ Synthesis

All procedures were performed under nitrogen using proper Schlenk line technique. 15 g of $CrCl_3 \cdot 6H_2O$ was dissolved in 30 mL of a 0.4 N sulfuric acid solution resulting in a dark green solution. Simultaneously 90 g of sodium acetate in 70 mL of H_2O was brought to a boil and bubbled with nitrogen for 30 min. The chromium solution was added to 10 g of zinc powder which was subjected to three vacuum/N_2 backfill cycles to remove any oxygen above the solution. After 45 minutes a deep blue solution was present which was diluted, via cannula transfer, with 190 mL of degassed H_2O. This was then rotated to allow the solution to filter through a fritted filter tube and drip into the sodium acetate solution, immediately brick red crystals began to form as the two

solutions mixed. This was allowed to stir overnight to ensure full precipitation of product. The product was filtered through a fritted filter tube, washed with 3 x 20 mL degassed H_2O and 3 x 20 mL degassed 200-proof ethanol. The filter tube was capped on one end and an adapter was used to apply a vacuum for 24 h to ensure total dryness of solid. The solid was transferred into an argon atmosphere glove box for storage. Yield 7.58 g, 71.6% A greater yield could be obtained from further precipitates in the filtrate, however to ensure purity only the material which was collected and washed on the frit was used for MOP syntheses. Due to the air sensitivity of Cr(II) ions, all syntheses and treatments of Cr-MOPs were performed in an Ar-filled glove box.

3.4.2.3 Synthesis of Cr-1

Isophthalic acid (100 mg) dissolved in 5 mL DEF and $Cr(OAc)_2$ (100 mg) in 10 mL DEF were mixed and placed in a 20 mL vial. The vial was sit in room temperature for 2 days. Purple block crystals of Cr-**1** were obtained. IR (ν max): 617, 694, 716, 744, 775, 812, 829, 910, 1026, 1109, 1201, 1269, 1367, 1566, 1598, 1726, 2312, 2372, 2864, 2962 cm^{-1}.

3.4.2.4 Synthesis of Cr-2

5-tert-butylisophthalic acid (200 mg) dissolved in 5 mL DMA and $Cr(OAc)_2$ (200 mg) in 10 mL DMA were mixed and placed in a 20 mL vial. The vial sat in room

Temp. for 2 days. Purple block crystals of Cr-**2** were obtained. IR (ν max): 623, 675, 696, 717, 746, 777, 810, 910, 949, 1012, 1058, 1188, 1265, 1354,1394, 1502, 1597, 1641, 1708, 2873, 2951 cm^{-1}.

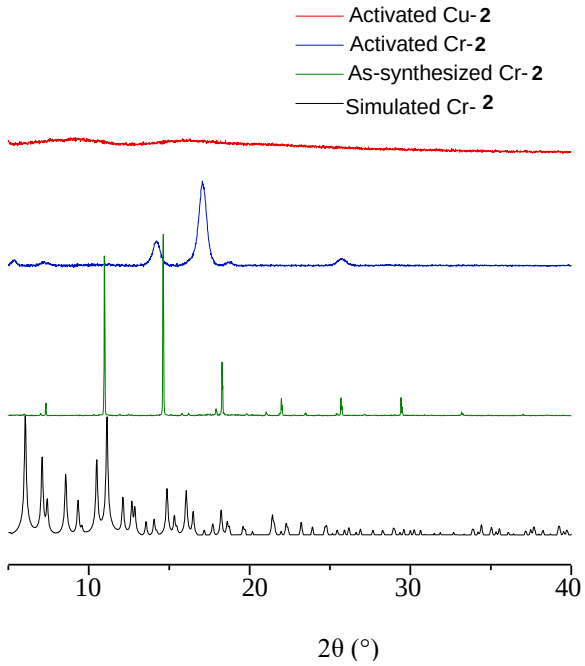

Figure 27 Powder diffraction patterns of Cr-2 and effects of activation on Cr-2 and Cu-2

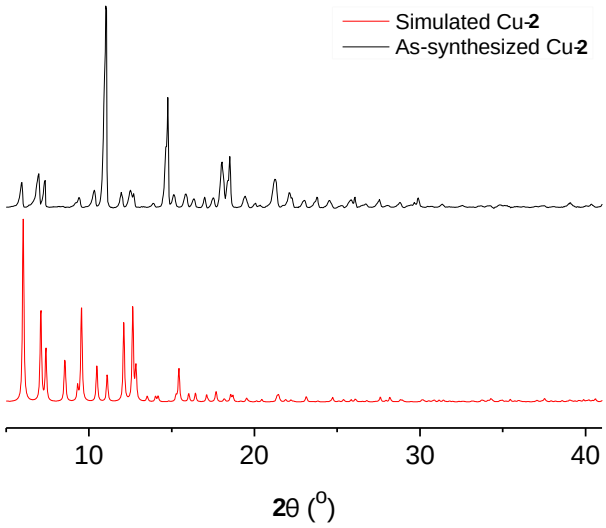

Figure 28 Powder X-ray diffraction pattern of Cu-2 (copper t-butyl isophthalate) and simulation of PXRD of Cu-2

3.4.2.5 Synthesis of Cr-3

For Cr-**3** in a rhombic space group, H_2TEI (100 mg) dissolved in 5 mL DEF and $Cr(OAc)_2$ (50 mg) in 10 mL DEF were mixed and placed in a 20 mL vial. The vial was sit in room temperature for 2 days. Purple diamond shape crystals of Cr-**3** were obtained. For Cr-**3** in a tetragonal space group, H_2TEI (100 mg) dissolved in 3 mL DEF and $Cr(OAc)_2$ (50 mg) in 5 mL DEF were mixed and placed in a 20 mL vial. The vial was allowed to sit at room temperature for 2 days. Purple octahedral shape crystals of Cr-**3** were obtained. IR (ν max): 671, 719, 771, 825, 881, 916, 962, 997,1012, 1072, 1103, 1130, 1211, 1247, 1271,1357,1427, 1564, 1625, 2152,2864, 2943 cm^{-1}.

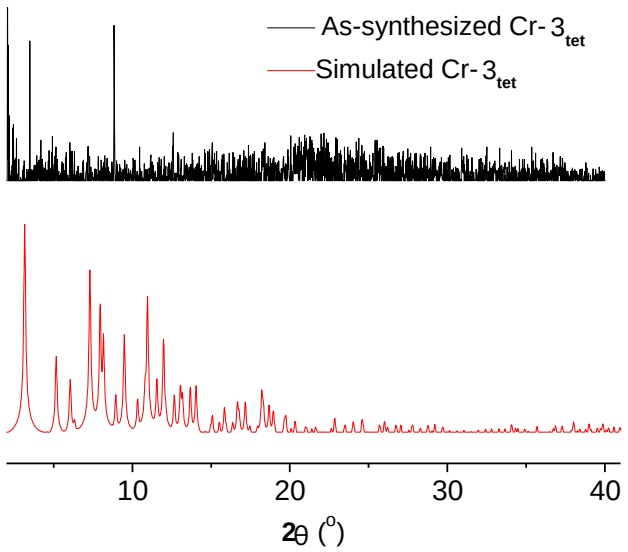

Figure 29 Powder X-ray diffraction pattern of Cr-3$_{tet}$ simulated and as synthesized

3.4.2.6 Synthesis of Cr-4

H_2Misoph (100 mg) along with 100 mg of chromous acetate were added to 10 mL DMA solution containing 100 mg of chromium acetate in a 20 mL scintillation vial. A stirbar was added and the solution mixed for 10 minutes and then removed from the glovebox and placed into an oven at 85 C for two days. Purple bar shaped crystals of Cr-**4** were obtained. Synthesis under similar conditions in DMA yielded octahedral shaped crystals but these could not be resolved via single-crystal x-ray diffraction. After activation at

200 °C for 12 hrs on a micromeritics ASAP 2020 at a maximum vacuum of 8 μbar 52.3 mg of tan solid was collected from the BET tube.

CHAPTER IV

STRUCTURAL CONTRIBUTIONS TO OBSERVED PACKING AND POROUS BEHAVIOR IN METAL-ORGANIC POLYHEDRA

4.1 Introduction

As has been demonstrated in this dissertation, work previously published by the Zhou group, [38-39, 41, 43, 45, 47, 136-137] the Yaghi group,[29-30, 138-139] and recent work published by the Bloch group[48-50, 93-94] paddlewheel based metal-organic polyhedra are a rich area of study for porous materials. However most of this previous work treats these molecular entities with two minds. One sees them entirely as molecular species and focus on the design of these discrete cages without considering how they will arrange in the solid state while the other treats them much like extended materials such as metal-organic frameworks and zeolites without properly considering how the pieces fit together. In the original publication of the first three chromium cages the experimental design largely fell into the latter category, relying on the known structure of the cages and viewing these materials as porous solids regardless of the local structure issues. To some extent it was thought that the most significant control in the experiments was the choice of cage topology. This is largely because many of these constructions, particularly neutral species such as paddle wheel based MOPs, are often insoluble once obtained in crystalline form. Thus the solids obtained, and characterized crystallographically, were assumed to be the only materials we could synthesize. Modifications made to increase solubility also increase the presence

of other problems such as structural characterization owing to the larger amount of disorder and less regular packing that is obtained in these species.[5, 18, 28, 32, 140-141] Often these works propose the usefulness of these structures lie in the possibility of solution-phase processing and further structural control not available to extended coordination polymers. Features such as solubility, facile synthesis, and further tunability are often sought but rarely observed for molecular coordination cages, this holds particularly true in the search for MOPs which can be used for gas storage and separations applications.[39, 47, 139] When these systems are reported they are generally not soluble except at elevated temperatures and in non-volatile solvents such as DMF. The TEI ligand, as discussed in Chapter III**,** provides both the copper and chromium MOPs with a wide solubility range in organic solvents at room temperature however the *tert*-Butyl isophthalic acid derivative shows no appreciable solubility. The molybdenum TBI MOP demonstrates through observed ligand exchange that it can be solubilized at elevated temperatures in amide solvents (DMF, DMA, DEF), but, a room temperature solution of it is not isolable as crystallization happens upon cooling.[112]

Synthesis of new MOP compounds is in many ways similar to the approach taken with metal-organic frameworks. Typically this requires a broad screening of solvents, concentrations, and other reaction variables to achieve high-quality single crystals or powders. This is necessary as formation of the cages is facile due to rapid ligand exchange and informed design principles, but, formation of the crystal requires regular order and a level of reversibility to reduce defects. In Metal-Organic Frameworks this is an absolute

necessity and achieving synthesis of only a single target phase, let alone a highly crystalline material, often requires hundreds of test reactions. One recurring concept that continues to drive researchers towards molecular porous materials is the possibility of ameliorating these problems through the solubility and surface functionality of discrete coordination complexes. This pushes the design of MOP based materials firmly into the area of crystal engineering. However, most of the literature on these cages focuses solely on the design and properties of the discrete cage rather than that of the resulting supramolecular-ordering of these species. While this may be a valid approach for investigating functionality in the solution phase and for applications such as sensing,[4] drug-delivery, and catalysis[4, 44, 95, 142] it is not sufficient for the study of porosity with respect to gas storage and separations.[4, 95, 143] As such a deeper discussion of the effects of solvents on MOP synthesis and structure, particularly with respect to the extended arrangements that arise in the crystalline state is needed.

4.1.1 Effects of synthesis conditions and functionality on MOP formation

Whereas the chromium MOPs, Cr-1-3, were successfully crystalized without applying heat and only a single solvent is used the other systems utilized more involved syntheses. This might be expected for the molybdenum species as the slower ligand exchange rate may necessitate applying a higher temperature and allowing a longer synthesis time, however the copper system, MOP-1 the first paddlewheel MOP published,[29] set a precedent that has generally been followed in the literature since. Closer inspection of the

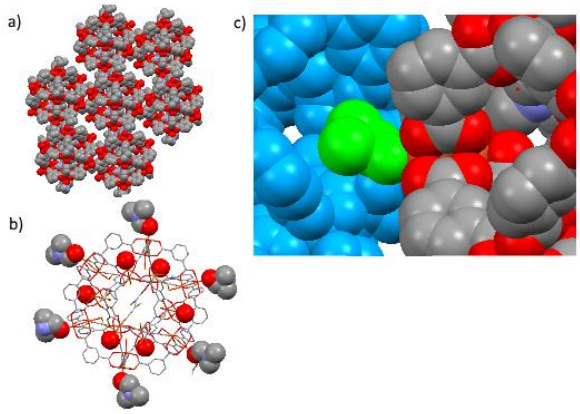

Figure 30 pseudo-hexagonal packing in MOP-1 and solvent participation in packing: a) single layer hexagonal packing viewing along c-axis, b) MOP-1 with exo solvents emphasized, c) nesting of exo-coordinated DMF (green) within the trianglular pore of an adjacent cage (blue)

structure of MOP-1 it is obvious that the solvents play a key role in the synthesis of the extended ordering in these materials (Figure 30).

The MOP-1 cages pack in pseudo-hexagonal sheets around the threefold axis through the trigonal caps at the center of the cuboctahedron (Figure 30a) In this structure by Eddoudi and co-workers the solvent molecules surrounding the cages were identified as six DMF molecules and six water molecule (Figure 30b). These DMF molecules are somewhat disordered but a clear pattern arises. The coordinated DMF molecule from one cage nests in the window of an adjacent cage. It was also found that upon standing it was found that a structural rearrangement had taken place. This resulted in the cages repacking in a body centered cubic motif and the space group changing to Im-3m (Figure 31a). This arrangement occurs due to the interlocking of the trigonal windows with the solvents

pointing towards the square windows. All coordinated solvents were assigned to water molecules but given the structure this is unlikely. Rather the DMF is likely disordered

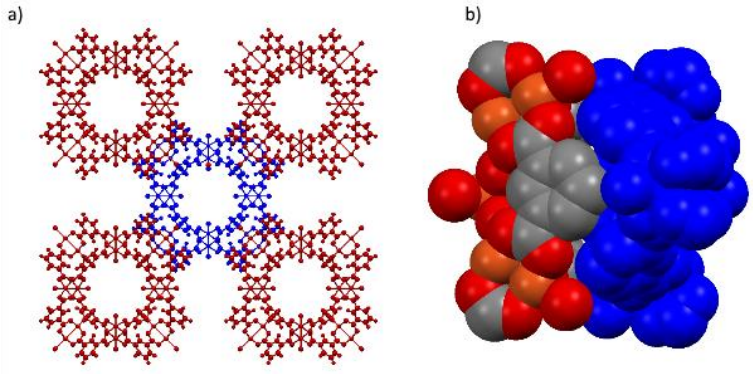

Figure 31 a) Body-centered cubic packing of MOP-1 in Im-3m and b) interlocking of trigonal windows

within the larger window/void spaces and cannot be resolved due to the higher symmetry of this crystal system. This is often an issue in the crystals of MOFs where large pores and metal nodes often sitting on sites of high symmetry resulting in an inability to resolve coordinated solvents. Rather than model the solvent within the void often only the atom directly coordinating the metal is resolved and the un-accounted for electron density in the pore is removed through a solvent mask or implementation of SQEEEZE. In MOFs this is usually accepted as a necessity since the disordered solvent can rarely be adequately resolved within the high symmetry space groups. This effect has carried over to MOPs and their reported structures. Though the voids within these systems tend to be smaller the high symmetry often leads to poor observation of solvents, coordinated or within the pores, and generally these are not considered when constructing new MOP crystals.

One case where intermolecular interactions were observed and taken advantage of is that the Zhou group with the the intent of studying the effects of photoisomerization and inducing photoswitchable gating of the pores, similar to what has been see in MOFs.[131, 140, 144-145] However, rather than controlled gating of pore access what was instead observed was reversible binding of an aromatic dye molecule, methylene blue, through control of MOP solubility. The ligands should be in present as the trans isomers under non-irradiative conditions and the MOP will not readily dissolve. This behavior was attributed to the intermolecular interactions of the extended azobenzene units (Figure 32c). When the dye was added the MOP absorbs it, which can be detected via UV-Vis spectroscopy. Upon irradiation the azobenzene contracts diminishing the intermolecular interactions and the cage and dye solubilize. This release of dye was measured by UV-Vis showing a slow release during irradiation (Figure 32d). This demonstrated the effects intermolecular interactions can have on MOP applications in the solution state and inspired further investigation of those effects in crystal design and in extension to the solid state.

This chapter focuses on the observed structural contributions in MOP material synthesis and observed behavior due to solvents and ligand functionalization. This is achieved through comparison of the structures, observed behavior, and characterization of previously published chromium(II) based MOPs (Cr-1, Cr-2, Cr-3) as well as further synthesis and structural characterization of new Cr(II) based MOP crystals using 5-methylisophthalic acid and 5-hydroxyisophthalic acid.

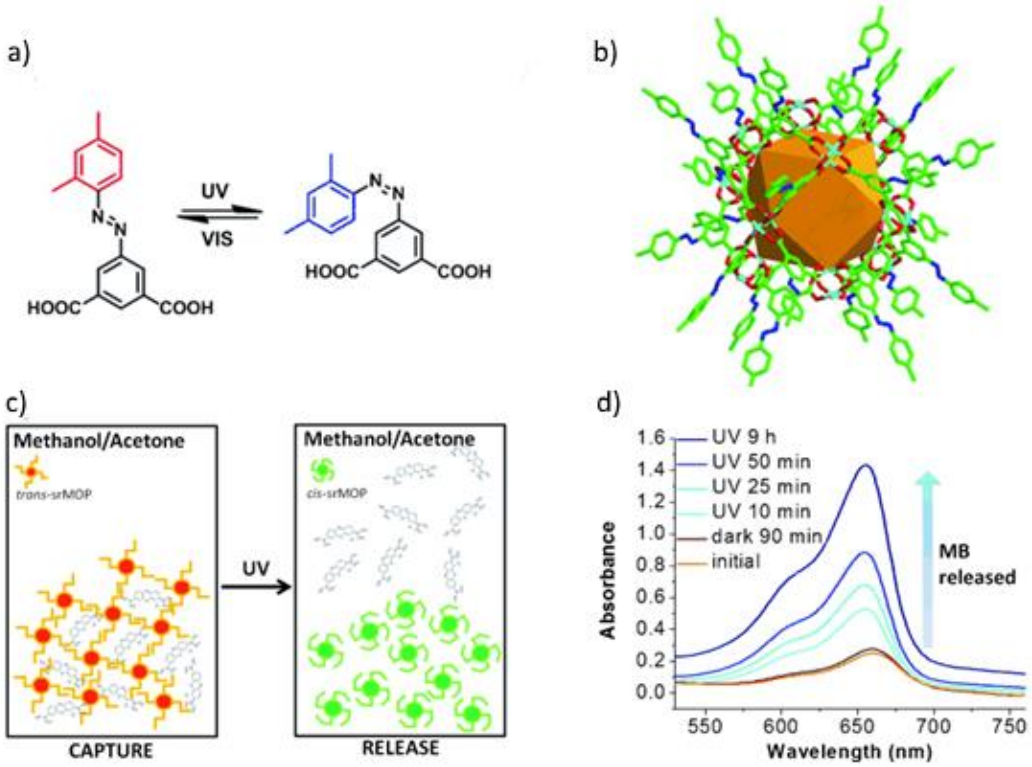

Figure 32 Azobenzene functionalized copper MOP a) azobenzene derived isophthalic acid ligand, b) MOP structure with azobenzenes in the trans-position, c) proposed mechanism for dye capture and release, the dye is trapped between azobenzene units in the precipitate (left) and is released upon radiation and isomerization (right) d) dye release during irradiation.[140]

4.2 Results and Discussion

4.2.1 Effects of Solvent on Synthesis of Cr(II) Metal-Organic Polyhedra Crystals

The preparation of the chromium(II) compounds discussed in this work largely differ from previous methods more typically employed in the synthesis of paddlewheel based MOPs.[17-18, 29, 35-36, 43, 109, 139-140] Perhaps the largest difference is that these MOPs are synthesized largely at room temperature from a solution consisting of only the solvent, ligand, and chromium(II) acetate dihydrate precursor. The molybdenum analogue is synthesized in a similar manner only using DMPU as the solvent but requiring several days of heating.[112] The published syntheses and resulting structures for the isophthalic acid MOPs of Cr(II), Mo(II), and Cu(II) were compared to determine if synthesis conditions played a role in the resulting crystal structures. While the cuboctahedral cages themselves are the same in terms of extended structure the packing between them is quite different owing to the solvent and synthesis conditions used.

Compared to MOP-1, the chromium analogue, Cr-1, shows similar behavior but the packing motif is different. Rather than hexagonal sheets or in a true body-centered cubic fashion Cr-1 packs in a tetragonally elongated body centered motif (Figure 33a). The structure was solved in the I4/m space group and only the oxygens of the solvent molecules directly coordinated to the metals were resolved. However a close inspection shows that the orientation of the paddlewheel nodes shows that the solvents must in fact rest within

the windows of adjacent cages (Figure 33b). This observation has also been made by Bloch

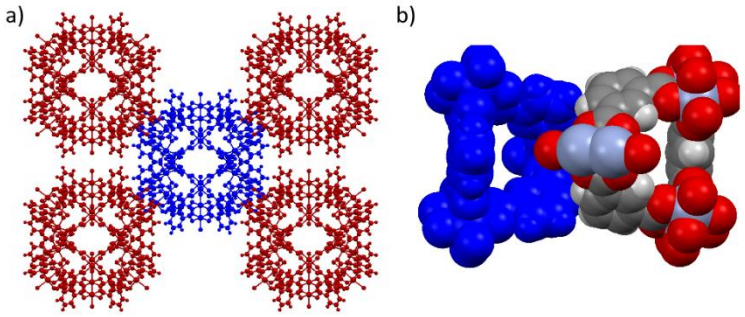

Figure 33 Tetragonally elongated body-centered packing of Cr-1 as viewed alon b-axis (a) and orientation of coordinated solvent towards triangular window of adjacent cage (b)

and coworkers in regards to the Cr(II) MOP formed by the 5-*tert*-Butylisophthalate (TBI) ligand.[49] In both cases for the isophthalate based cages the phenyl rings from adjacent cages sit against one another at a distance of ~3.8 A from carbon to adjacent carbon in a side on fashion. Additionally while MOP-1 packs via solvent "bridging" from

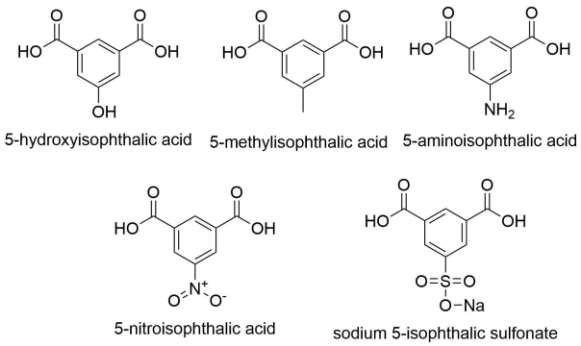

Figure 34 5-substituted isopthalic acid ligands used for investigation of new Cr(II) MOPs

coordination in one cage to the square pores of the adjacent cage Cr-1 is packed via bridging from chromium center to the adjacent triangular window. The molybdenum isophthalate species behaves similarly with the chromium, however, the larger DBU ligands rest in the square windows of adjacent cages as shown in Figure 35.[39] This alignment blocks the pores and gives an arrangement without long-range channels as discussed seen in the chromium materials.

Since thermal activation of these materials typically decomposes the copper MOPs whilst the porosity of the chromium MOPs is achieved only at high (>180 °C) temperatures further structural investigation of the role of coordinated solvents in cuboctahedra cages is warranted. A series of cuboctahedral cages synthesized under various solvent and thermal conditions were investigated to determine the structural factors that controlled relative orientation of the cages within the extended solids.

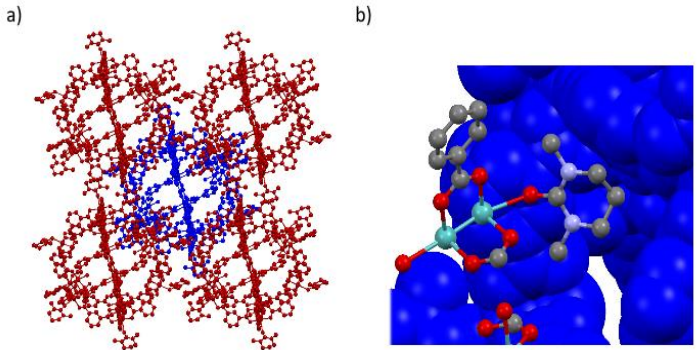

Figure 35 Molybdenum isopthalate cage packing (a) and DMPU resting in the square pore window (b)

The series of chromium MOPs previously reported (Cr-1-3)[47], those structures reported by the Bloch group[49, 94, 141], as well as new chromium MOP ligands were chosen for the investigation (Figure 34). To ensure that the structures would be comparable to previous work and to one another 5- substituted isophthalic acid ligands were chosen. The intention in choosing these ligands was to modulate the resulting cage structures through interactions of the ligands. By choosing ligands that would have stronger intermolecular interactions, such as through hydrogen bonding, it was hypothesized that the structural stability of these materials could be improved during the activation process. However

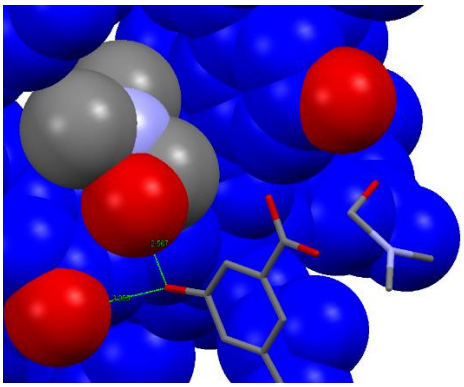

Figure 36 Hydroxyl groups hydrogen bonding to one another and adjacent DMF binding in pore window

single crystals were only obtained for the methyl and hydroxyl derivatives with the hydroxyl containing ligand giving different crystal packing depending on the temperature of synthesis (Figure 37c and f).

The amino derivative did occasionally yield what appeared to be small, droplet shaped crystals but these did not diffract. Solutions containing both chromium(II) acetate and 5-amino-isophthalic acid turned turbid and no crystalline material was obtained at room or elevated temperatures. This is possibly due to the amino group coordinating in the axial position either of the starting material or adjacent cages. The nitro derivative yielded almost immediate, within 2-5 minutes, formation of a blue sol-gel of the entire solution. Likewise the sulfonate derivative, depending on reaction conditions, yielded fine powders or gels. While the isostructural copper and molybdenum MOPs are known, no crystals large enough for single crystal diffraction were obtained with chromium. Attempts to obtain powder diffraction data were unsuccessful, largely due to oxidation issues. The material was activated utilizing the scheme previously employed resulted in decomposition yielding a gray-green powder and no significant porosity. It is hypothesized that while the ligand itself is known to be thermally stable it may not be in proximity to such strong reducing agents at 200 °C. There was however success in obtaining crystals of the methyl and hydroxyl derivatives yielding the first single crystal structures of these MOPs, Cr-4 and Cr-5 respectively.

The hydroxyl derivative had been previously synthesized by Bloch but the single crystal structure was not obtained.[49] Two different crystal packing modes were obtained via syntheses at room temp, space group R_1 Cr-5_{Rhom}, and 85 °C, space group I4/m Cr-5_{tet}. The structure obtained in I4/m is a good fit for the unit-cell parameters, a = b = 28.4653(17)

Å c = 41.067(3) Å α = β = γ = 90° for Cr-5_{tet}, determined by Bloch of a = b = 29.42 Å and c = 41.18 Å α = β = γ = 90° in either I4/m or P4/mm space groups. While the crystal

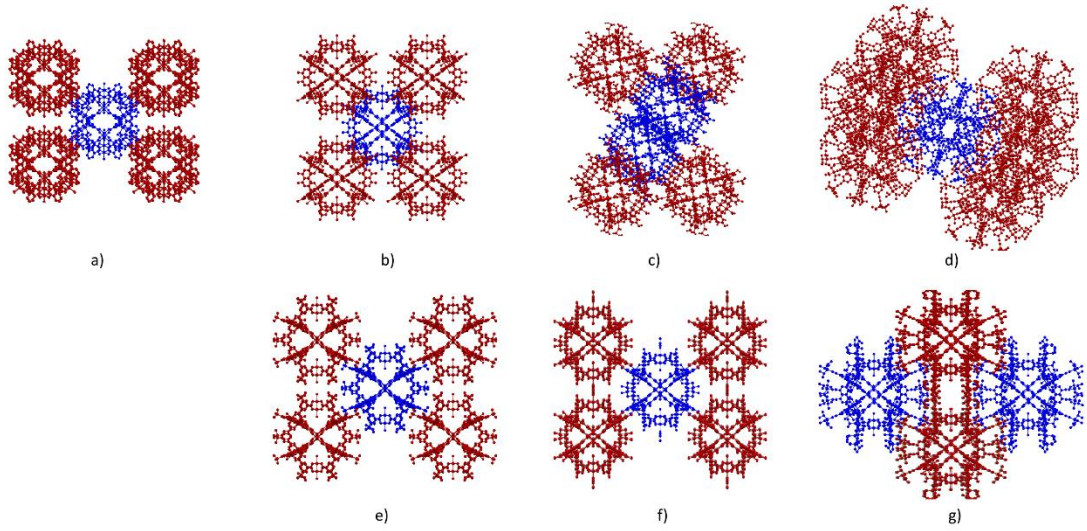

Figure 37 Packing motifs of chromium MOPs a) Cr-1 b) Cr-5_{rhom} c) Cr-4 d) Cr-3_{rhom} e) Cr-2 f) Cr-5_{tet} g) Cr-3_{tet}. Red and blue used to identify crystallographically distinct cages

quality is rather poor the structure can be resolved to show that the packing between the cages is due entirely to interactions between coordinated solvents (Figure 37c). It was expected that in this cage the hydroxyl groups might interact in a similar manner to that of the *t*-Butyl ligand forming three fold arrangements through hydrogen bonding. The large voids between the cages and poor data quality mean that the solvents in the pore-volume cannot be resolved though based on the structure of Cr-5_{rhom} they may play a role as well. Unlike Cr-5_{tet} the crystal structure of 5_{rhom} shows clear indications of participation of the hydroxyl groups in the formation of the extended structure (Figure 37f). The

hydroxyl groups from each ligand show evidence of hydrogen bonding with a hydroxyl group of the adjacent cage. Further the hydroxyl group also is within range to indicate the

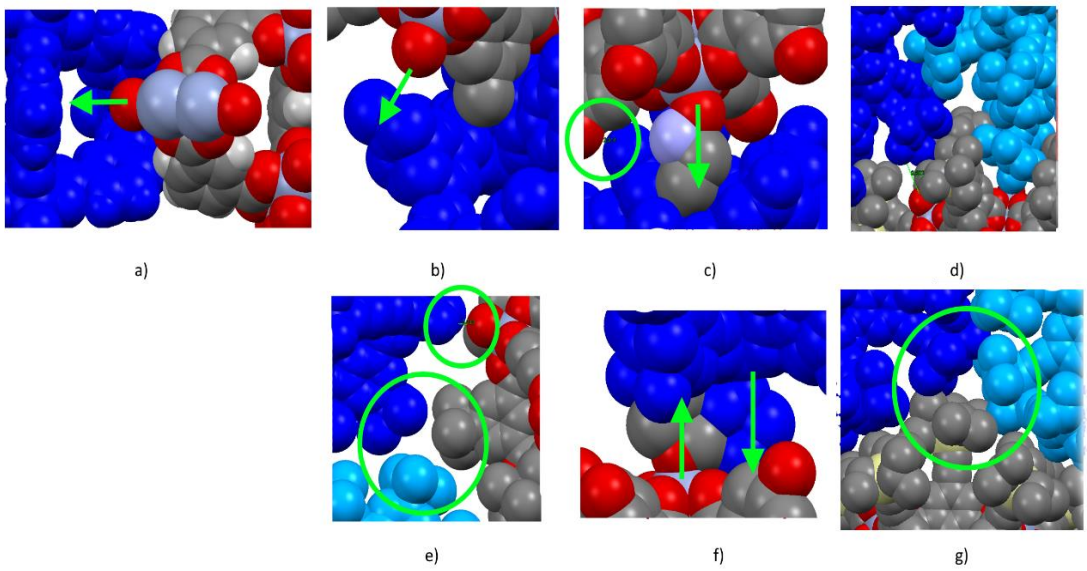

Figure 38 Interactions between chromium(II) cages that generate observed packing motifs a) solvent pointing towards neighboring pore(green arrow) in Cr-1, b) methyl group resting in neighboring pore and solvent pointing to neighboring pore, c) hydrogen bonding between hydroxyl groups (green circle) and solvent resting in neighboring pore in Cr-5$_{rhom}$, d) interdigitation of triisopropylsilyl groups in Cr-3$_{rhom}$, e) trigonal arrangement of t-butyl groups (lower circle) and close spacing of solvents (top circle) in Cr-2, f) side by side interactions of coordinated solvents in Cr-5$_{tet}$, g) trigonal arrangement of triisopropylsilyl groups in Cr-3$_{tet}$

possibility of hydrogen bonding, ~3.2 A, to the carbonyl of a DMF molecule which occupies the triangular window of the neighboring MOP. This is in contrast to what is seen in many of the other cages wherein the coordinated solvents directly bridge the cages either by resting within an adjacent window or directly interacting with one another such

as in Cr-1 or Cr-5_{tet} respectively. The general packing schemes for each of the cages discussed in this chapter are shown in Figure 37.

4.2.2 Role of Solvents in Cage Packing

There are obvious patterns in the packing seen in Figure 37 for each of the MOPs. Particularly the alignment of the metal centers with the pore windows in most of these extended cage arrangements is highlighted in the observed packing. This is largely due to the solvents used in these syntheses as compared to previous synthesis of related cages with other metals. This is frequently driven by coordinated solvent molecules extending from the exo-position of one paddlewheel into a pore window of an adjacent MOP. This is possible due to the relatively small size of the dimethyl or diethyl amine groups found in these solvents. This is readily observed by looking at the discrete interactions within these structures in Figure 38. As previously discussed the isophthalate MOP packs through the extension of coordinated solvent molecules into the triangular windows of adjacent cages. This gives rise to the tetragonally elongated body-centered packing of the cages where each of the four top and bottom paddlewheels coordinate a solvent which interlocks with one of eight triangular windows in the adjacent eight cages. Additionally the phenyl rings of the ligand rest against one another in a side on fashion. In the example of the molybdenum isophthalate cage described earlier in this chapter rather than packing towards the triangular windows, the larger DMPU directs the paddlewheels to point towards the more spacious square windows.[39] This is possibly due to the lack of other

directing groups on the MOP backbone. It has been shown that when the group in the 5-position of these ligands is elongated such as alkoxy groups of various lengths that they can coil within the windows for the best fit.[141] In the copper isophthalate example it is seen that while the larger DMF solvent directs the alignment of paddlewheel and pore it's absence yields a higly symmetric window to window packed structure due to the tight fitting of the phenyl rings (Figure 31). Such arrangements are impossible or exceedingly unlikely for functionalized isopthalates because competing interactions will prevent such structures from occurring.

The methyl derivative, Cr-4 (Figure 38b), has this solvent interaction but rather than the solvent in the triangular windows it is the methyl group that nests within them. The solvents instead point into the inter-cage void spaces. Cr-4 is the only cage in this series that packs in this manner though other paddlewheel cages pack in this way it is usually only seen when the ligand has a moiety that is close in size to the size of the cage windows.[17, 30, 34, 36, 39] While the crystals of Cr-4 showed no solublity in DMF, DMA, or DEF they do have considerable solubility in *N*,*N*-Diethyl-*m*-toluamide (DEET). This was taken advantage of to obtain the first solution state UV-Vis of a chromium(II) cuboctahedral cage (*vida infra*).

The *tert*-Butyl derivative Cr-2, Figure 38e, which has a similar but larger functionality packs through a trigonal arrangement of the tert-butyl groups of three adjacent cages. This arrangement and packing motif is seen in most of the examples of cuboctahedra utilizing

this ligand including the copper,[47] molybdenum,[39] and ruthenium[114] analogs. This interaction is also seen in the Cr-3_{tet} packing arrangement (Figure 38g) indicating that it is observable when bulky groups are present as compared to those which allow a closer approach or can rest within the pore windows. Cr-3_{rhom} however shows an interdigitation of the triisopropyl silyl groups. It is not known why these two different structures are obtained with the only synthetic difference being the concentration, however it is postulated that the tetragonal packing is due to the higher concentration precipitating out what might be considered the kinetic product of crystallization. Once these crystals are present they serve as seeds to control the phase of the resulting material. While MOPs are generally considered to be the kinetic products in these syntheses, rather than MOFs or 2-D coordination polymers which occur often in the Cu(II) analogs at elevated temperatures, the formation of the extended structure must also have kinetic and thermodynamic considerations in formation.

The formation of the cages can be exceedingly quick, the copper(II) 5-hydroxy-isophthalate cuboctahedral MOP assembles in less than a minute from mixing to formation of the paddlewheel and fragment condensation to the resulting cage in methanol.[146] Even if formation of the related chromium species takes longer due to higher solvent viscosity or slower exchange kinetics for the chromium(II) acetate to the isophthalate ligand the reaction will be complete long before the several days required to obtain crystals has passed. The study of the crystallization nucleation and growth conditions will need to be addressed in future work, however, it is relevant to what is observed for both Cr-3 and Cr-

5 as two distinct crystallographic packing structures are obtained through varying synthetic conditions. Previously only the MOP-1 structure was reported with two separate crystallographic forms from such similar synthesis conditions and that only due to the crystals being allowed to sit for some months before reanalysis.[33]

The structure of Cr-5 in both rhombohedral and tetragonal space groups is controlled through interactions between the hydroxyl groups (Figure 38c and f respectively), however, these are very different than that seen from the TEI ligand. The packing in the Cr-5_{rhom} structure is due to three sets of interactions: 1) hydroxyl groups between the cages form hydrogen bond linkages (Figure 36 and green circle Figure 38), 2) coordinated solvent bridges from the metal centers to an adjacent window (green arrow Figure 38c), and 3) hydrogen bonding between the hydroxyl groups and solvent molecules resting in other pore windows (Figure 36). The large number of interactions between the cages and relatively close packing might explain the observed heavy level of twinning, occurring almost exclusively at right angles. If a cage were to rotate 90° the only way to continue the packing pattern is in that direction thus nucleation of new crystals may occur due to multiple directions the cages can pack. The tetragonal packing however is very similar to that seen in the other MOPs and is directed largely by solvent interactions rather than the hydroxyl groups. The cages in this motif do not pack as tightly as rather than direct cage to cage interactions or solvent to cage interactions the coordinated solvents align with one another in pointing into the adjacent pores. With the solvents sitting on top of each other the cages cannot approach as closely as they do with some of the other functionalities.

Other solvents in the void spaces could not be resolved but it is also likely that these play a role, along with the large DMA solvent, in achieving this structure. The larger solvent and heating allow the reversible aggregation of the cages which yields higher quality crystals. This lead to the investigation of other related solvents that might take advantage of such effects.

4.2.3 Solvation of Chromium(II) MOPs

After taking a deeper look at the crystal structures and the impacts solvents play a variety of new synthetic conditions were applied to try and grow new MOP structures. DEET, a major component of mosquito repellants, came to my attention as a possible solvent. DEET has a structure much like the amide solvents commonly applied in these syntheses (Figure 39). The large DEET molecule has both the steric bulk of DEF with the additional *m*-tolyl group. When coordinated to a metal center through the carbonyl this molecule will not readily fit inside of the pore windows of adjacent cages but would pack well with itself. The hope then was that this would provide crystal structures which could be easily dissolved, however, this did not work as anticipated. The chromous acetate is not appreciably soluble in DEET at room temperature at the concentrations typically employed in these syntheses. Instead once the solution is saturated a thick gel-like layer forms at the bottom of the container it is being mixed in. Thus room temperature syntheses were not successful for either chromium or copper. Crystals were found in the copper samples but were found to be recrystallized copper acetate and

unreacted ligand. In most cases where a reaction was observed at room temperature or 85 °C only gels were obtained. However, at elevated temperatures it was found that in certain cases no precipitate formed at temperature or even upon cooling. This was especially true utilizing the methyl ligand which for copper yielded a deep blue solution.

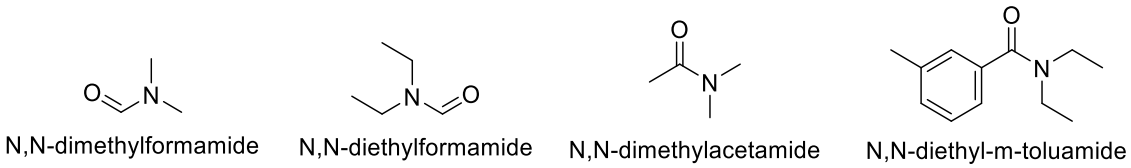

Figure 39 Amide based solvents commonly used in MOP and MOF synthesis compared to DEET

Attempts to generate crystals via addition of precipitating solvents (water, acetonitrile, diethylether) from this stock solution were unsuccessful producing either no observable reaction besides dilution, more gels, cloudy precipitates and colloidal suspensions which remain suspended for weeks to months. Taking crystals of Cr-4 that had been solvent exchanged with DMF for 1 day and adding DEET with subsequent stirring dissolved and formed a solution that showed no precipitate over six months. Similar to the copper cage no crystals were able to be grown from this solution. This however did present an opportunity to take UV-Vis measurements of a dichromium cage for the first time. While it would have been possible to take UV-VIS during synthesis due to the quick formation of the cages the presence of residual acetate, and any resulting equilibrium, would have complicated the spectra. The washing step allowed removal of excess

acetate that may have remained from the synthesis. Comparing the spectra of Cr-5 and chromous acetate in DEET shows some similarities and differences (Figure 40).

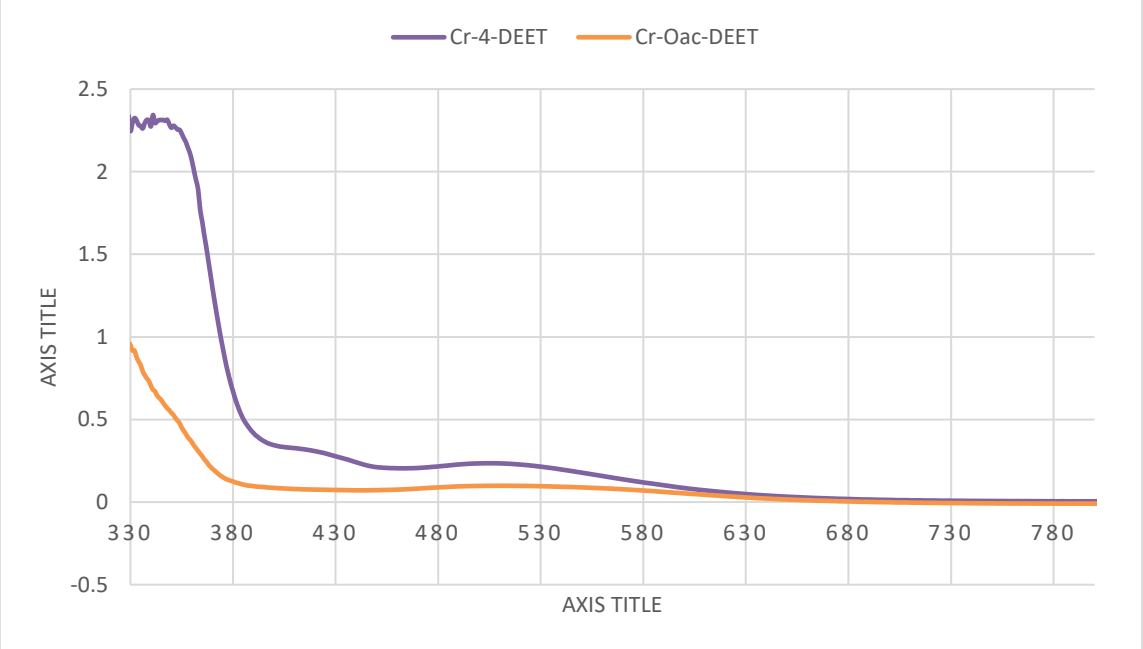

Figure 40 UV-Visible spectrum of Cr-4 (purple) dissolved in DEET and chromous acetate (yellow) in DEET

Chromium(II) acetate shows a peak at 330 nm but due and another broad peak centered at 524 nm closely matching reported values. In comparison the ~330 nm peak for cage Cr-4 cannot be interpreted due to saturation of the detector. The rise of a peak at 424 nm and a broad feature centered at 512 nm are also apparent for the cage. The acetate in DEET has similar absorbances as the two features reported for chromium acetate monohydrate of 476 nm and 333 nm.[147] The differences may arise due to the DEET

coordination of the paddlewheel. The additional peak for the cage may arise from the presences of an aryl ligand and the bridging nature of the ligand. The few chromium(II) carboxylate paddlewheels synthesized with aryl ligands do not report electronic spectra so there is not much literature for comparison.[116, 148-149] In reevaluating the literature and

Figure 41 Cr-2 after activation in toluene (left) and after oxidation by air (right)

specifically the previously discussed report of a non-axially coordinated chromium(II) carboxylate paddle wheel, in the writing of this dissertation the solubility of that compound stood out. The triisopropylbenzoic acid ligands (Figure 23) and the bulk they provided enabled the compound to be soluble in non-polar solutions. The idea that the *tert*-Butyl groups on Cr-2 might enable a similar solubility emerged. Taking a sample of already activated Cr-2, 61 mg, and adding 10 mL of toluene gave a cloudy yellow solution. Centrifugation of this solution gave a mostly clear yellow-orange solution with a fine brown solid as shown in Figure 41. This was encouraging as the cage as synthesized and generally all other carboxylate bridged Cr(II) paddle wheels are brick

red to dark purple in color. However the previously reported unaxially coordinated species was orange-yellow. This also presented the opportunity to obtain the second reported UV-Vis spectrum of a potentially unaxially coordinated chromium carboxylate paddle wheel. The UV-Vis spectra of activated Cr-2 in toluene and with the additions of acetonitrile and triphenylphosphine are shown in Figure 42.

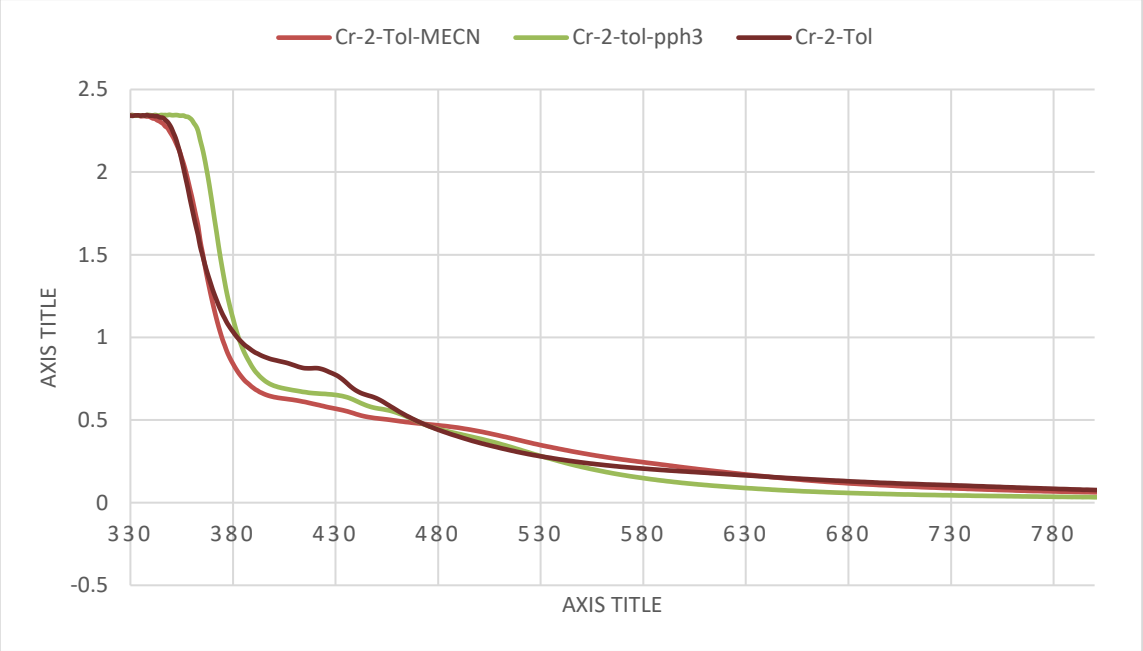

Figure 42 UV-Visible spectrum of Cr-2 in toluene (Purple), Cr-2 in toluene + acetonitrile (red), Cr-2 in toluene + triphenylphosphine (green)

The same broad peak present in Cr-4 is seen for all three samples however the as dissolved Cr-2 and the acetonitrile added sample show two new features in the area of ~430 to 450

nM. The peaks for Cr-2 in toluene are 427 nm and 452 nm almost identical to the 453 nm and 423 nm peaks reported for the unaxially coordinated paddle wheel previously.[104]

The acetonitrile added sample approaches that seen of Cr-4 in DEET indicating coordination of the axial positions. This spectrum was taken after only several minutes of sitting and thus may not reflect a fully equilibrated sample. Triphenyl phosphine was selected as a dopant as its larger size might have prevented diffusion into the pores and it can be see than it still maintains two peaks at approximately 330 nm and 360 nm. This data is highly preliminary and attribution of these peaks to specific transitions is made here. To ensure that oxidation was not causing the shifts the samples were opened to air and air was forced through them by a pipette until no further color change could be detected Figure 43. As can be seen in the figure above oxidation greatly reduces the uptake of any peaks at 330 nm and a new peak at ~585 nm is observed in all three samples. This peak is diagnostic of the oxidation of the chromous acetate and is not seen in the previous spectra indicating that oxidation, if occurring, is not what is being observed. Cr-4 still shows some absorption at 330 nm which may be due to a secondary

product or due to the higher viscosity and nature of the cage preventing full oxidation in the time between collecting data. Additionally while both samples in DEET remain in solution the sample in toluene precipitates as a fluffy green material. This is attributed to the poor solvating effect toluene would have for the oxidized chromium species. In the absence of other ligands the decomposed cages likely aggregate. This is further evidence

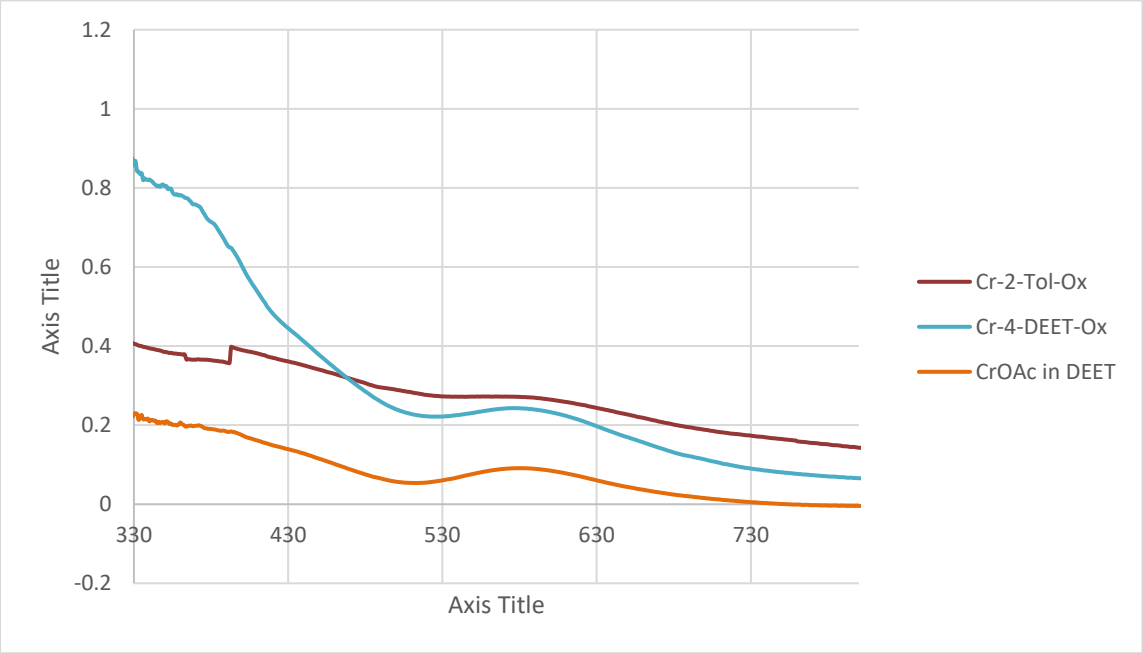

Figure 43 UV-VIS spectrum of oxidized chromium species Cr-2 in Tol (Blue), Cr-4 in DEET (red), and chromium(II) acetate dihydrate (Orange)

for the proposed hypothesis that the molecular nature of these cages is why they are not as stable to oxygen binding as other 3-D systems. While the data presented here is very preliminary the ability to observed and potentially isolate the unaxially solvated cages is an opportunity to access a previously undeveloped area of chemistry.

4.3 Future Work

4.3.1 Control of cage packing through solvent size analysis

Based on the observations in this dissertation of the inter-cage interactions that drive packing in porous MOP materials there should be a systematic study completed utilizing a variety of solvents with various steric properties to develop a practical methodology for predicting cage packing and orientation. While the insights provided here give direction future work should consider the quantification of packing effects through computational and experimental methods. This will enable the creation of a set of crystal engineering rules on which researchers can consistently rely. This could be accomplished by screening solvents, functional group size and identity, temperatures, and several different metals and then comparing the resulting crystal structures. Through a combination of high-throughput computation and high-throughput automated synthetic methods these samples could be readily collected and analyzed for property-function relationships for each piece of the design puzzle.

Through such a study it may also be possible to identify the dividing line between extended structure stability and pore stability in the copper systems. By carefully controlling the inter-cage interaction strength, and tuning functionality such that solvent plays a less involved role in packing, generation of highly porous copper MOP based materials may be realized.

4.3.2 Control of uncoordinated cage packing through functional group control

Through the discovery that the activated cages can potentially be accessed post-synthesis through solution chemistry a new series of highly-reactive coordination structures is now accessible. Further work should seek to isolate and crystalize these cages which, could then be activated under less strenuous conditions. This gives the potential to have these materials activated without structural aggregation. The use of larger functional groups and non-coordinating solvents will be required to prevent further aggregation. Once these cages are isolated a new series of compounds can be generated by creating asymmetrically coordinated paddle wheels through ligand size control. The use of large ligands would limit coordination to only the exo-position of the cages leaving the internal position open and potentially more reactive. This can be applied to the chromium cages for investigation in improving interactions with gases such as methane and hydrogen. The synthesis of the V(II) analogs may provide even stronger interactions. It may even be possible to use these systems as porous liquids through control of solvent size and solubility.

Perhaps even more interesting is that this may be applied to other metals such as rhodium and ruthenium paddle wheels. The generation of asymmetric ligation as well as size exclusion properties of these cages may enable new catalytic activities from readily synthesized MOPs.

4.4 Experimental

4.4.1 Instrumentation and Materials

4.4.1.1 Instrumentation

UV-Vis was measured on a Shimadzu spectrometer from 330-1100 nm at the fast scan setting.

4.4.1.2 Chemicals

All chemicals were used as received. Solvents were purchased from EMD-milipore and were dried and degassed prior to use. 5-methylisophthalic and sodium 5-isophthalica acid sulfonate were purchased from Sigma-Aldrich and 5-hydroxyisophthalic acid, 5-aminoisophthalic acid, and 5-nitroisophthalic acid were purchased from TCI.

4.4.2 Synthesis

4.4.2.1 Chromium(II) acetate monohydrate

Was synthesized according to the procedure in Chapter III

4.4.2.2 Cr-1,2,3,4

Crystals of crystallographic quality of MOPs Cr 1-4 were synthesized according to the procedures in Chapter III

4.4.2.3 Cr-5_{Rhom}

Cr-5_{rhom} was prepared in an analogous manner to the other chromium(II) MOP materials. 200mg of $Cr_2(OAc)_4 \cdot 2H_2O$ and 200 mg of 5-hydroxyisophthalic acid were dissolved in DMF and stirred for 10 minutes in a 20 mL scintillation vial. This solution was allowed to sit for two days over which time highly twinned deep purple/red rod shaped crystals up to 3mm in length of the product were formed.

4.4.2.4 Cr-5_{Tet}

Cr-5_{Tet} was prepared in an analogous manner to the other chromium(II) MOP materials. 200mg of $Cr_2(OAc)_4 \cdot 2H_2O$ and 200 mg of 5-hydroxyisophthalic acid were dissolved in DMA and stirred for 10 minutes in a 20 mL scintillation vial. The vial was tightly capped and removed from the glovebox then placed in an oven at 85 °C. This solution was allowed to sit for two days over which time large purple octahedral shaped crystals of the product were formed. While consistent control of crystal size was difficult occasionally crystals over 1mm on an edge were obtained in this manner.

4.4.2.5 Other ligand screening

For the amino, nitro, and sodium sulfonate functionalized ligands crystal growth was screened through conditions of 8-15 mg/mL of ligand and 10-20 mg/mL of either cupric or chromous acetate at room temperature, 65 °C, and 85 °C in DMF, DMA, and DEET. The nitro ligand yielded blue gels within minutes under all conditions indicating that the ligand was oxidizing the chromium. The molybdenum version of this cage is known however. Under pure solvent conditions single crystals of x-ray quality were never achieved. Several of the copper reactions had what appeared to be crystals but they decomposed on the synchrotron beamline and no data was successfully collected locally.

4.4.3 Uv-Vis Characterization

4.4.3.1 UV-Visible spectrum of chromium(II) acetate and Cr-4 in DEET

To prepare a dilute enough sample 0.1 ml of saturated chromous acetate in DEET was added to five ml of DEET to dilute. The cage solution was prepared by dissolving the products of one vial of Cr-4 in 10 mL of DEET. 1 ml of this solution was added to 2 ml of neat DEET for the UV-Vis measurements. The oxidized spectra were collected after removing the septum and forcing air through the solution in the cuvette via a pipette until no further color change could be detected.

4.4.3.2 UV-Visible spectrum of Cr-2 and its solvent adducts in toluene

To prepare a solution for UV-Vis measurements 61 mg of activated Cr-2, which had a slight discoloration after several months in the glovebox, was added to a vial along with 10 ml of dry toluene. Given the timeline of the realization that this experiment could be performed this was the only sample available for analysis prior to completion of this dissertation. This solution was stirred overnight giving a cloudy yellow solution then removed from the box and centrifuged giving a clear yellow solution. This was then placed back in the glovebox to prepare the samples. For the cage itself 1 ml of the prepared solution was added to the cuvette along with 2 ml of dry toluene. For the acetonitrile adduct .14 ml of acetonitrile was added to the solution through the septum of the cuvette. The oxidized spectrum for this sample was collected after removing the septum and forcing air through the solution in the cuvette via a pipette until no further color change could be detected. The PPh_3 adduct solution was made the night before the measurement by taking 1 ml of the mother solution and adding an excess of PPh_3 allowing it to sit. This was diluted using 2 ml of neat toluene. Dilution with either heptane or chlorobenzene caused some precipitation but no crystal formation was observed.

CHAPTER V

CONCLUSIONS

5.1 Porous Polymers in Carbon Capture

The research presented here shows that new routes towards porous materials for carbon capture are an active area of study with many avenues to investigate. The benzimidazole porous polymer PPN-1 showed initial promise in carbon capture applications but more recent investigations and a better understanding of the scope has led me to believe that it was never as competitive as it was originally purported to be. While it was competitive in the chemical literature the original study did not consider the current practical conditions under which such systems operate. This was typical in the literature at the time but as the field has broadened an appreciation for the engineering challenges and requirements for such systems has been impressed upon the materials science discipline. As such the investigation of systems with alkyl amines appended or structurally included within the backbone remain the best class of materials for such research. There also remains a lag between what systems engineers are designing as next generation systems and what materials scientists are designing and next generation sorbents. Over my studies it has become obvious that this gap, while lessened, still exists to a significant degree and serves as a major impediment to transformational changes in these technologies. Federal funders have taken note and now require more applied components to new sorbent research systems. This is a positive trend and should it continue new

transformational sorbent systems should appear within the literature in the next few years and hopefully in power plants within the next fifteen.

5.2 Metal-Organic Polyhedra as Porous Materials

The continued activity in the study of Metal-Organic Polyhedra is a sign of a bevy of advancements to come. However, accessing these materials as solid sorbents still has much room to grow. The chromium MOPs discussed in this these advance that area of study in two ways. First they demonstrate that larger architectures constructed from coordination bonds can maintain porosity even under more extreme conditions. Secondly their inherent stability allows for the study of the other structural factors that are normally occluded by instability in the copper(II) examples that dominate the literature. The work that needs to be accomplished here is to take a few steps back from the gas adsorption and take a more holistic view of the synthesis of these materials. The focus on the individual cages has previously limited accessibility of porosity in these systems as the long-rang ordering was not being controlled. If such materials are going to be viewed the same as other extended coordination structures like MOFs and zeolites then the forces that hold them together can no longer be taken for granted. Though works have tried to account for these factors they are often looking at other applications than gas sorption.[107]

The realization that the non-axially coordinated cages are accessible through solvation opens up an even broader range of possibilities. While this behavior has been observed in these chromium systems the extension of this to the rhodium, molybdenum, and ruthenium systems may allow for new chemistries to be identified. Taking advantage of the structural control over the cages new size and shape selective host-guest systems may be devised to observe previously unobservable phenomena. While the failures to obtain a broader range of materials in the course of this work is unfortunate the observations that could be made from those that were successful and those that weren't provides a path forward to obtaining new materials in a more facile manner.

To achieve such results researchers must consider the cage topology, size of windows or clefts in the cage surface and how these compare to ligand functionalities and solvents. If solvent is similar in size to cage windows it will likely rest there if it is too large then functional groups might rest in the windows. If both are large then the cages align at the functional groups, such as in the TEI, MOPs. By preselecting solvent size or including competing ligands/molecules it may be possible to control material phase.

The work in chapters II and III is in many ways preliminary but without analyzing the current set of results further progress had been stymied. Future work in this area is open to a number of possibilities and with the considerations made here hopefully new experiments can be developed to take full advantage of metal-organic polyhedra with

full synthetic design from metal and ligand choice to cage topology and ultimately to the control of the three-dimensional arrangement of the cages.

REFERENCES

1. Makal, T. A.; Li, J. R.; Lu, W.; Zhou, H. C., Methane storage in advanced porous materials. *Chem Soc Rev* **2012,** *41* (23), 7761-79.

2. Medishetty, R.; Zareba, J. K.; Mayer, D.; Samoc, M.; Fischer, R. A., Nonlinear optical properties, upconversion and lasing in metal-organic frameworks. *Chem Soc Rev* **2017,** *46* (16), 4976-5004.

3. Zou, L.; Sun, Y.; Che, S.; Yang, X.; Wang, X.; Bosch, M.; Wang, Q.; Li, H.; Smith, M.; Yuan, S.; Perry, Z.; Zhou, H. C., Porous Organic Polymers for Post-Combustion Carbon Capture. *Adv Mater* **2017,** *29* (37), 1700229.

4. Ahmad, N.; Younus, H. A.; Chughtai, A. H.; Verpoort, F., Metal-organic molecular cages: applications of biochemical implications. *Chem Soc Rev* **2015,** *44* (1), 9-25.

5. Ahmad, N.; Chughtai, A. H.; Younus, H. A.; Verpoort, F., Discrete metal-carboxylate self-assembled cages: Design, synthesis and applications. *Coordination Chemistry Reviews* **2014,** *280*, 1-27.

6. Han, M.; Engelhard, D. M.; Clever, G. H., Self-assembled coordination cages based on banana-shaped ligands. *Chem Soc Rev* **2014,** *43* (6), 1848-60.

7. Mason, J. A.; Veenstra, M.; Long, J. R., Evaluating metal–organic frameworks for natural gas storage. *Chem. Sci.* **2014,** *5* (1), 32-51.

8. Han, Y.; Li, J.-R.; Xie, Y.; Guo, G., Substitution Reactions in Metal-Organic Frameworks and Metal-Organic Polyhedra. *Chem. Soc. Rev.* **2014,** *43* (16), 5952-5981.

9. Cook, T. R.; Zheng, Y.-R.; Stang, P. J., Metal-Organic Frameworks and Self-Assembled Supramolecular Coordination Complexes: Comparing and Contrasting the Design, Synthesis, and Functionality of Metal-Organic Materials. *Chemical Reviews* **2013,** *113* (1), 734-777.

10. Sumida, K.; Rogow, D. L.; Mason, J. A.; McDonald, T. M.; Bloch, E. D.; Herm, Z. R.; Bae, T. H.; Long, J. R., Carbon dioxide capture in metal-organic frameworks. *Chem Rev* **2012,** *112* (2), 724-81.

11. Lu, W. G.; Yuan, D. Q.; Zhao, D.; Schilling, C. I.; Plietzsch, O.; Muller, T.; Brase, S.; Guenther, J.; Blumel, J.; Krishna, R.; Li, Z.; Zhou, H. C., Porous Polymer Networks: Synthesis, Porosity, and Applications in Gas Storage/Separation. *Chemistry of Materials* **2010,** *22* (21), 5964-5972.

12. Sekizkardes, A. K.; Kusuma, V. A.; Dahe, G.; Roth, E. A.; Hill, L. J.; Marti, A.; Macala, M.; Venna, S. R.; Hopkinson, D., Separation of carbon dioxide from flue gas by mixed matrix membranes using dual phase microporous polymeric constituents. *Chem Commun (Camb)* **2016,** *52* (79), 11768-11771.

13. Yuan, D.; Lu, W.; Zhao, D.; Zhou, H. C., Highly stable porous polymer networks with exceptionally high gas-uptake capacities. *Adv Mater* **2011,** *23* (32), 3723-5.

14. Guillerm, V.; Kim, D.; Eubank, J. F.; Luebke, R.; Liu, X.; Adil, K.; Lah, M. S.; Eddaoudi, M., A supermolecular building approach for the design and construction of metal-organic frameworks. *Chem Soc Rev* **2014,** *43* (16), 6141-72.

15. Zhang, M. W.; Chen, Y. P.; Zhou, H. C., Structural design of porous coordination networks from tetrahedral building units. *Crystengcomm* **2013,** *15* (45), 9544-9552.

16. Cook, T. R.; Zheng, Y.-R.; Stang, P. J., Metal–Organic Frameworks and Self-Assembled Supramolecular Coordination Complexes: Comparing and Contrasting the Design, Synthesis, and Functionality of Metal–Organic Materials. *Chemical Reviews* **2013,** *113* (1), 734-777.

17. Tranchemontagne, D. J.; Ni, Z.; O'Keeffe, M.; Yaghi, O. M., Reticular chemistry of metal-organic polyhedra. *Angew Chem Int Ed Engl* **2008,** *47* (28), 5136-47.

18. Han, Y.; Li, J. R.; Xie, Y.; Guo, G., Substitution reactions in metal-organic frameworks and metal-organic polyhedra. *Chem Soc Rev* **2014,** *43* (16), 5952-81.

19. Cote, A. P.; Benin, A. I.; Ockwig, N. W.; O'Keeffe, M.; Matzger, A. J.; Yaghi, O. M., Porous, crystalline, covalent organic frameworks. *Science* **2005,** *310* (5751), 1166-70.

20. Lu, W.; Sculley, J. P.; Yuan, D.; Krishna, R.; Wei, Z.; Zhou, H. C., Polyamine-tethered porous polymer networks for carbon dioxide capture from flue gas. *Angew Chem Int Ed Engl* **2012,** *51* (30), 7480-4.

21. Zhang, M. W.; Perry, Z.; Park, J.; Zhou, H. C., Stable benzimidazole-incorporated porous polymer network for carbon capture with high efficiency and low cost. *Polymer* **2014,** *55* (1), 335-339.

22. Yang, X. Y.; Zou, L. F.; Zhou, H. C., Anchor installation on porous polymer networks (PPNs) for high CO_2 uptake. *Polymer* **2017,** *126*, 303-307.

23. Islamoglu, T.; Behera, S.; Kahveci, Z.; Tessema, T. D.; Jena, P.; El-Kaderi, H. M., Enhanced Carbon Dioxide Capture from Landfill Gas Using Bifunctionalized Benzimidazole-Linked Polymers. *ACS Appl Mater Interfaces* **2016,** *8* (23), 14648-55.

24. Deutsch, E.; Taube, H., Acetopentaaquochromium(III) ion. *Inorg. Chem.* **1968,** *7*, 1532.

25. Northrop, B. H.; Zheng, Y. R.; Chi, K. W.; Stang, P. J., Self-organization in coordination-driven self-assembly. *Acc Chem Res* **2009,** *42* (10), 1554-63.

26. Li, H.; Eddaoudi, M.; O'Keeffe, M.; Yaghi, O. M., Design and synthesis of an exceptionally stable and highly porous metal-organic framework. *Nature* **1999,** *402* (6759), 276-279.

27. Chui, S. S.-Y.; Lo, S. M.-F.; Charmant, J. P. H.; Orpen, A. G.; Williams, I. D., A Chemically Functionalizable Nanoporous Material $[Cu_3(TMA)_2(H_2O)_3]$. *Science* **1999,** *283* (5405), 1148-1150.

28. Cook, T. R.; Zheng, Y. R.; Stang, P. J., Metal-organic frameworks and self-assembled supramolecular coordination complexes: comparing and contrasting the design, synthesis, and functionality of metal-organic materials. *Chem Rev* **2013,** *113* (1), 734-77.

29. Eddaoudi, M.; Kim, J.; Wachter, J. B.; Chae, H. K.; O'Keeffe, M.; Yaghi, O. M., Porous Metal-Organic Polyhedra: 25 Å Cuboctahedron Constructed from 12 $Cu_2(CO_2)_4$ Paddle-Wheel Building Blocks. *J. Am. Chem. Soc.* **2001,** *123*, 4368.

30. Sudik, A. C.; Millward, A. R.; Ockwig, N. W.; Cote, A. P.; Kim, J.; Yaghi, O. M., Design, synthesis, structure, and gas (N_2, Ar, CO_2, CH_4, and H_2) sorption properties of porous metal-organic tetrahedral and heterocuboidal polyhedra. *J Am Chem Soc* **2005,** *127* (19), 7110-8.

31. Fujita, M.; Yazaki, J.; Ogura, K., Preparation of a macrocyclic polynuclear complex, $[(en)Pd(4,4'\text{-bpy})]_4(NO_3)_8$ (en = ethylenediamine, bpy = bipyridine), which recognizes an organic molecule in aqueous media. *J. Am. Chem. Soc.* **1990,** *112*, 5645.

32. Furukawa, H.; Kim, J.; Ockwig, N. W.; O'Keeffe, M.; Yaghi, O. M., Control of Vertex Geometry, Structure Dimensionality, Functionality, and Pore Metrics in the Reticular Synthesis of Crystalline Metal–Organic Frameworks and Polyhedra. *J. Am. Chem. Soc.* **2008,** *130*, 11650.

33. Eddaoudi, M.; Kim, J.; Wachter, J. B.; Chae, H. K.; O'Keeffe, M.; Yaghi, O. M., Porous Metal−Organic Polyhedra: 25 Å Cuboctahedron Constructed from 12 Cu2(CO2)4 Paddle-Wheel Building Blocks. *Journal of the American Chemical Society* **2001,** *123* (18), 4368-4369.

34. Ke, Y.; Collins, D. J.; Zhou, H. C., Synthesis and structure of cuboctahedral and anticuboctahedral cages containing 12 quadruply bonded dimolybdenum units. *Inorg Chem* **2005,** *44* (12), 4154-6.

35. Park, J.; Chen, Y. P.; Perry, Z.; Li, J. R.; Zhou, H. C., Preparation of core-shell coordination molecular assemblies via the enrichment of structure-directing "codes" of bridging ligands and metathesis of metal units. *J Am Chem Soc* **2014,** *136* (48), 16895-901.

36. Young, M. D.; Zhang, Q.; Zhou, H. C., Metal-organic polyhedra constructed from dinuclear ruthenium paddlewheels. *Inorganica Chimica Acta* **2015,** *424*, 216-220.

37. Perry, J. J.; Perman, J. A.; Zaworotko, M. J., Design and synthesis of metal-organic frameworks using metal-organic polyhedra as supermolecular building blocks. *Chemical Society Reviews* **2009,** *38* (5), 1400-1417.

38. Li, J. R.; Zhou, H. C., Metal–Organic Hendecahedra Assembled from Dinuclear Paddlewheel Nodes and Mixtures of Ditopic Linkers with 120 and 90° Bend Angles. *Angew. Chem., Int. Ed.* **2009,** *48*, 8465.

39. Li, J. R.; Yakovenko, A. A.; Lu, W.; Timmons, D. J.; Zhuang, W.; Yuan, D.; Zhou, H. C., Ligand bridging-angle-driven assembly of molecular architectures based on quadruply bonded Mo-Mo dimers. *J Am Chem Soc* **2010,** *132* (49), 17599-610.

40. Furukawa, S.; Horike, N.; Kondo, M.; Hijikata, Y.; Carné-Sánchez, A.; Larpent, P.; Louvain, N.; Diring, S.; Sato, H.; Matsuda, R.; Kawano, R.; Kitagawa, S., Rhodium–Organic Cuboctahedra as Porous Solids with Strong Binding Sites. *Inorganic Chemistry* **2016,** *55* (21), 10843-10846.

41. Liu, T. F.; Chen, Y. P.; Yakovenko, A. A.; Zhou, H. C., Interconversion between discrete and a chain of nanocages: self-assembly via a solvent-driven, dimension-augmentation strategy. *J Am Chem Soc* **2012,** *134* (42), 17358-61.

42. Li, J.-R.; Zhou, H.-C., Bridging-ligand-substitution strategy for the preparation of metal–organic polyhedra. *Nat Chem* **2010,** *2* (10), 893-898.

43. Sun, L. B.; Li, J. R.; Lu, W.; Gu, Z. Y.; Luo, Z.; Zhou, H. C., Confinement of metal-organic polyhedra in silica nanopores. *J Am Chem Soc* **2012,** *134* (38), 15923-8.

44. Kang, Y. H.; Liu, X. D.; Yan, N.; Jiang, Y.; Liu, X. Q.; Sun, L. B.; Li, J. R., Fabrication of Isolated Metal-Organic Polyhedra in Confined Cavities: Adsorbents/Catalysts with Unusual Dispersity and Activity. *J Am Chem Soc* **2016,** *138* (19), 6099-102.

45. Jiang, Y.; Park, J.; Tan, P.; Feng, L.; Liu, X. Q.; Sun, L. B.; Zhou, H. C., Maximizing Photoresponsive Efficiency by Isolating Metal-Organic Polyhedra into Confined Nanoscaled Spaces. *J Am Chem Soc* **2019,** *141* (20), 8221-8227.

46. Sudik, A. C.; Millward, A. R.; Ockwig, N. W.; Côté, A. P.; Kim, J.; Yaghi, O. M., Design, Synthesis, Structure, and Gas (N_2, Ar, CO_2, CH_4, and H_2) Sorption Properties of Porous Metal-Organic Tetrahedral and Heterocuboidal Polyhedra. *J. Am. Chem. Soc.* **2005,** *127* (19), 7110-7118.

47. Park, J.; Perry, Z.; Chen, Y. P.; Bae, J.; Zhou, H. C., Chromium(II) Metal-Organic Polyhedra as Highly Porous Materials. *ACS Appl Mater Interfaces* **2017,** *9* (33), 28064-28068.

48. Bloch, E. D.; Queen, W. L.; Krishna, R.; Zadrozny, J. M.; Brown, C. M.; Long, J. R., Hydrocarbon separations in a metal-organic framework with open iron(II) coordination sites. *Science* **2012,** *335* (6076), 1606-10.

49. Lorzing, G. R.; Trump, B. A.; Brown, C. M.; Bloch, E. D., Selective Gas Adsorption in Highly Porous Chromium(II)-Based Metal–Organic Polyhedra. *Chemistry of Materials* **2017,** *29* (20), 8583-8587.

50. Rowland, C. A.; Lorzing, G. R.; Gosselin, E. J.; Trump, B. A.; Yap, G. P. A.; Brown, C. M.; Bloch, E. D., Methane Storage in Paddlewheel-Based Porous Coordination Cages. *J Am Chem Soc* **2018,** *140* (36), 11153-11157.

51. Cychosz, K. A.; Thommes, M., Progress in the Physisorption Characterization of Nanoporous Gas Storage Materials. *Engineering* **2018,** *4* (4), 559-566.

52. Ambroz, F.; Macdonald, T. J.; Martis, V.; Parkin, I. P., Evaluation of the BET Theory for the Characterization of Meso and Microporous MOFs. *Small Methods* **2018,** *2* (11), 1800173.

53. Pearson, P. N.; Palmer, M. R., Atmospheric carbon dioxide concentrations over the past 60 million years. *Nature* **2000,** *406* (6797), 695-9.

54. Wriedt, M.; Sculley, J. P.; Yakovenko, A. A.; Ma, Y.; Halder, G. J.; Balbuena, P. B.; Zhou, H. C., Low-energy selective capture of carbon dioxide by a pre-designed elastic single-molecule trap. *Angew Chem Int Ed Engl* **2012,** *51* (39), 9804-8.

55. Sculley, J. P.; Verdegaal, W. M.; Lu, W.; Wriedt, M.; Zhou, H. C., High-throughput analytical model to evaluate materials for temperature swing adsorption processes. *Adv Mater* **2013,** *25* (29), 3957-61.

56. Davis, M. E., Ordered porous materials for emerging applications. *Nature* **2002,** *417* (6891), 813-21.

57. Zhou, H. C.; Long, J. R.; Yaghi, O. M., Introduction to metal-organic frameworks. *Chem Rev* **2012,** *112* (2), 673-4.

58. Yuan, D.; Zhao, D.; Sun, D.; Zhou, H. C., An isoreticular series of metal-organic frameworks with dendritic hexacarboxylate ligands and exceptionally high gas-uptake capacity. *Angew Chem Int Ed Engl* **2010,** *49* (31), 5357-61.

59. Ma, S.; Sun, D.; Wang, X. S.; Zhou, H. C., A mesh-adjustable molecular sieve for general use in gas separation. *Angew Chem Int Ed Engl* **2007,** *46* (14), 2458-62.

60. Li, H.; Wang, K.; Feng, D.; Chen, Y. P.; Verdegaal, W.; Zhou, H. C., Incorporation of Alkylamine into Metal-Organic Frameworks through a Bronsted Acid-Base Reaction for CO2 Capture. *ChemSusChem* **2016,** *9* (19), 2832-2840.

61. Mason, J. A.; Sumida, K.; Herm, Z. R.; Krishna, R.; Long, J. R., Evaluating metal–organic frameworks for post-combustion carbon dioxide capture via temperature swing adsorption. *Energy & Environmental Science* **2011,** *4* (8), 3030-3040.

62. Ben, T.; Ren, H.; Ma, S.; Cao, D.; Lan, J.; Jing, X.; Wang, W.; Xu, J.; Deng, F.; Simmons, J. M.; Qiu, S.; Zhu, G., Targeted synthesis of a porous aromatic framework with high stability and exceptionally high surface area. *Angew Chem Int Ed Engl* **2009,** *48* (50), 9457-60.

63. Lu, W.; Yuan, D.; Sculley, J.; Zhao, D.; Krishna, R.; Zhou, H. C., Sulfonate-grafted porous polymer networks for preferential CO_2 adsorption at low pressure. *J Am Chem Soc* **2011,** *133* (45), 18126-9.

64. McDonald, T. M.; Lee, W. R.; Mason, J. A.; Wiers, B. M.; Hong, C. S.; Long, J. R., Capture of carbon dioxide from air and flue gas in the alkylamine-appended metal-organic framework mmen-Mg_2(dobpdc). *J Am Chem Soc* **2012,** *134* (16), 7056-65.

65. Lu, W.; Bosch, M.; Yuan, D.; Zhou, H. C., Cost-effective synthesis of amine-tethered porous materials for carbon capture. *ChemSusChem* **2015,** *8* (3), 433-8.

66. Zou, L. F.; Yang, X. Y.; Yuan, S.; Zhou, H. C., Flexible monomer-based covalent organic frameworks: design, structure and functions. *Crystengcomm* **2017,** *19* (33), 4868-4871.

67. Zhu, X.; Tian, C.; Mahurin, S. M.; Chai, S. H.; Wang, C.; Brown, S.; Veith, G. M.; Luo, H.; Liu, H.; Dai, S., A superacid-catalyzed synthesis of porous membranes based on triazine frameworks for CO_2 separation. *J Am Chem Soc* **2012,** *134* (25), 10478-84.

68. Ren, S.; Bojdys, M. J.; Dawson, R.; Laybourn, A.; Khimyak, Y. Z.; Adams, D. J.; Cooper, A. I., Porous, fluorescent, covalent triazine-based frameworks via room-temperature and microwave-assisted synthesis. *Adv Mater* **2012,** *24* (17), 2357-61.

69. Kou, Y.; Xu, Y.; Guo, Z.; Jiang, D., Supercapacitive energy storage and electric power supply using an aza-fused pi-conjugated microporous framework. *Angew Chem Int Ed Engl* **2011,** *50* (37), 8753-7.

70. Asensio, J. A.; Sanchez, E. M.; Gomez-Romero, P., Proton-conducting membranes based on benzimidazole polymers for high-temperature PEM fuel cells. A chemical quest. *Chem Soc Rev* **2010,** *39* (8), 3210-39.

71. Rabbani, M. G.; El-Kaderi, H. M., Template-Free Synthesis of a Highly Porous Benzimidazole-Linked Polymer for CO_2 Capture and H_2 Storage. *Chemistry of Materials* **2011,** *23* (7), 1650-1653.

72. Fournier, J.-H.; Wang, X.; Wuest, J. D., Derivatives of tetraphenylmethane and tetraphenylsilane: Synthesis of new tetrahedral building blocks for molecular construction. *Canadian Journal of Chemistry* **2003,** *81* (5), 376-380.

73. Chen, L.; Kim, J.; Ishizuka, T.; Honsho, Y.; Saeki, A.; Seki, S.; Ihee, H.; Jiang, D., Noncovalently netted, photoconductive sheets with extremely high carrier mobility and conduction anisotropy from triphenylene-fused metal trigon conjugates. *J Am Chem Soc* **2009,** *131* (21), 7287-92.

74. Pariya, C.; Marcos, Y. S.; Zhang, Y.; Fronczek, F. R.; Maverick, A. W., Organosilicon-Based Multifunctional β-Diketones and their Rhodium and Iridium Complexes. *Organometallics* **2008,** *27* (17), 4318-4324.

75. Suh, M. P.; Park, H. J.; Prasad, T. K.; Lim, D. W., Hydrogen storage in metal-organic frameworks. *Chem Rev* **2012,** *112* (2), 782-835.

76. Altarawneh, S.; Islamoglu, T.; Sekizkardes, A. K.; El-Kaderi, H. M., Effect of acid-catalyzed formation rates of benzimidazole-linked polymers on porosity and selective CO2 capture from gas mixtures. *Environ Sci Technol* **2015,** *49* (7), 4715-23.

77. Rabbani, M. G.; El-Kaderi, H. M., Synthesis and Characterization of Porous Benzimidazole-Linked Polymers and Their Performance in Small Gas Storage and Selective Uptake. *Chemistry of Materials* **2012,** *24* (8), 1511-1517.

78. Sekizkardes, A. K.; Culp, J. T.; Islamoglu, T.; Marti, A.; Hopkinson, D.; Myers, C.; El-Kaderi, H. M.; Nulwala, H. B., An ultra-microporous organic polymer for high performance carbon dioxide capture and separation. *Chem Commun (Camb)* **2015,** *51* (69), 13393-6.

79. Rabbani, M. G.; Sekizkardes, A. K.; El-Kadri, O. M.; Kaafarani, B. R.; El-Kaderi, H. M., Pyrene-directed growth of nanoporous benzimidazole-linked nanofibers and their application to selective CO_2 capture and separation. *Journal of Materials Chemistry* **2012,** *22* (48), 25409-25417.

80. Shan, M.; Seoane, B.; Pustovarenko, A.; Wang, X.; Liu, X.; Yarulina, I.; Abou-Hamad, E.; Kapteijn, F.; Gascon, J., Benzimidazole linked polymers (BILPs) in mixed-matrix membranes: Influence of filler porosity on the CO_2/N_2 separation performance. *Journal of Membrane Science* **2018,** *566*, 213-222.

81. Day, G. S., Drake, H. F., Joseph, E. A., Bosch, M., Tan, Jui, Willman, J.A., Carretier, V., Perry, Z., Burtner, W., Banerjee, S. Ozdemir, O. K., Zhou, H.-C., Improving alkyl-amine incorporation in porous polymer networks through dopant incorporation. *Under Review* **2019**.

82. Tan, M. X.; Zhang, Y.; Ying, J. Y., Mesoporous poly(melamine-formaldehyde) solid sorbent for carbon dioxide capture. *ChemSusChem* **2013,** *6* (7), 1186-90.

83. Long, J. R.; Yaghi, O. M., The Pervasive Chemistry of Metal-Organic Frameworks. *Chem. Soc. Rev.* **2009,** *38* (5), 1213-1214.

84. Tranchemontagne, D. J.; Ni, Z.; O'Keeffe, M.; Yaghi, O. M., Reticular Chemistry of Metal-Organic Polyhedra. *Angew. Chem. Int. Ed.* **2008,** *47* (28), 5136-5147.

85. Perry Iv, J. J.; Perman, J. A.; Zaworotko, M. J., Design and Synthesis of Metal-Organic Frameworks Using Metal-Organic Polyhedra as Supermolecular Building Blocks. *Chem. Soc. Rev.* **2009,** *38* (5), 1400-1417.

86. Ahmad, N.; Younus, H. A.; Chughtai, A. H.; Verpoort, F., Metal-Organic Molecular Cages: Applications of Biochemical Implications. *Chem. Soc. Rev.* **2015,** *44* (1), 9-25.

87. Ahmad, N.; Chughtai, A. H.; Younus, H. A.; Verpoort, F., Discrete Metal-Carboxylate Self-Assembled Cages: Design, Synthesis and Applications. *Coord. Chem. Rev.* **2014,** *280* (0), 1-27.

88. Han, M.; Engelhard, D. M.; Clever, G. H., Self-Assembled Coordination Cages based on Banana-Shaped Ligands. *Chem. Soc. Rev.* **2014,** *43* (6), 1848-1860.

89. Zhai, Q.-G.; Mao, C.; Zhao, X.; Lin, Q.; Bu, F.; Chen, X.; Bu, X.; Feng, P., Cooperative Crystallization of Heterometallic Indium–Chromium Metal-Organic Polyhedra and Their Fast Proton Conductivity. *Angew. Chem. Int. Ed.* **2015,** *54* (27), 7886-7890.

90. Chen, L.; Reiss, P. S.; Chong, S. Y.; Holden, D.; Jelfs, K. E.; Hasell, T.; Little, M. A.; Kewley, A.; Briggs, M. E.; Stephenson, A.; Thomas, K. M.; Armstrong, J. A.; Bell, J.; Busto, J.; Noel, R.; Liu, J.; Strachan, D. M.; Thallapally, P. K.; Cooper, A. I., Separation of Rare Gases and Chiral Molecules by Selective Binding in Porous Organic Cages. *Nat. Mater.* **2014,** *13* (10), 954-960.

91. Mitra, T.; Jelfs, K. E.; Schmidtmann, M.; Ahmed, A.; Chong, S. Y.; Adams, D. J.; Cooper, A. I., Molecular Shape Sorting Using Molecular Organic Cages. *Nat. Chem.* **2013,** *5* (4), 276-281.

92. Furukawa, H.; Kim, J.; Ockwig, N. W.; O'Keeffe, M.; Yaghi, O. M., Control of Vertex Geometry, Structure Dimensionality, Functionality, and Pore Metrics in the Reticular Synthesis of Crystalline Metal−Organic Frameworks and Polyhedra. *J. Am. Chem. Soc.* **2008,** *130* (35), 11650-11661.

93. Bloch, E. D.; Queen, W. L.; Hudson, M. R.; Mason, J. A.; Xiao, D. J.; Murray, L. J.; Flacau, R.; Brown, C. M.; Long, J. R., Hydrogen Storage and Selective, Reversible O_2 Adsorption in a Metal-Organic Framework with Open Chromium(II) Sites. *Angew Chem Int Ed Engl* **2016,** *55* (30), 8605-9.

94. Gosselin, E. J.; Lorzing, G. R.; Trump, B. A.; Brown, C. M.; Bloch, E. D., Gas adsorption in an isostructural series of pillared coordination cages. *Chem Commun (Camb)* **2018,** *54* (49), 6392-6395.

95. Lu, W.; Yuan, D.; Yakovenko, A.; Zhou, H. C., Surface functionalization of metal-organic polyhedron for homogeneous cyclopropanation catalysis. *Chem Commun (Camb)* **2011,** *47* (17), 4968-70.

96. Li, J.-R.; Zhou, H.-C., Metal–Organic Hendecahedra Assembled from Dinuclear Paddlewheel Nodes and Mixtures of Ditopic Linkers with 120 and 90° Bend Angles. *Angew. Chem. Int. Ed.* **2009,** *48* (45), 8465-8468.

97. Sun, L. B.; Li, J. R.; Lu, W.; Gu, Z. Y.; Luo, Z.; Zhou, H. C., Confinement of Metal-Organic Polyhedra in Silica Nanopores. *J. Am. Chem. Soc.* **2012,** *134*, 15923-15928.

98. Kang, Y.-H.; Liu, X.-D.; Yan, N.; Jiang, Y.; Liu, X.-Q.; Sun, L.-B.; Li, J.-R., Fabrication of Isolated Metal-Organic Polyhedra in Confined Cavities: Adsorbents/Catalysts with Unusual Dispersity and Activity. *J. Am. Chem. Soc.* **2016,** *138* (19), 6099-6102.

99. Qiu, X.; Zhong, W.; Bai, C.; Li, Y., Encapsulation of a Metal-Organic Polyhedral in the Pores of a Metal-Organic Framework. *J. Am. Chem. Soc.* **2016,** *138*, 1138-1141.

100. Guillerm, V.; Kim, D.; Eubank, J. F.; Luebke, R.; Liu, X.; Adil, K.; Lah, M. S.; Eddaoudi, M., A Supermolecular Building Approach for the Design and Construction of Metal-Organic Frameworks. *Chem. Soc. Rev.* **2014,** *43* (16), 6141-6172.

101. Peskov, M. V.; Miao, X.-H.; Heryadi, D.; Eppinger, J.; Schwingenschlögl, U., Electronic and Magnetic Properties of Infinite 1D Chains of Paddlewheel Carboxylates $M_2(COOR)_4$ (M = Mo, W, Ru, Rh, Ir, Cu). *J. Phys. Chem. C* **2013,** *117* (10), 5462-5469.

102. Cotton, F. A.; Rice, C. E.; Rice, G. W., Crystal and Molecular Structure of Anhydrous Tetraacetatodichromium. *J. Am. Chem. Soc.* **1977,** *99* (14), 4704-4707.

103. Cotton, F. A.; Hillard, E. A.; Murillo, C. A.; Zhou, H.-C., After 155 Years, a Crystalline Chromium Carboxylate with a Supershort Cr−Cr Bond. *Journal of the American Chemical Society* **2000,** *122* (2), 416-417.

104. Cotton, F. A.; Hillard, E. A.; Murillo, C. A.; Zhou, H. C., After 155 Years, a Crystalline Chromium Carboxylate with a Supershort Cr–Cr Bond. *J. Am. Chem. Soc.* **2000,** *122*, 416.

105. Cotton, F. A.; Rice, C. E.; Rice, G. W., Crystal and Molecular-Structure of Anhydrous Tetraacetatodichromium. *Journal of the American Chemical Society* **1977,** *99* (14), 4704-4707.

106. Prakash, M. J.; Zou, Y.; Hong, S.; Park, M.; Bui, M. P.; Seong, G. H.; Lah, M. S., Metal-organic polyhedron based on a Cu(II) paddle-wheel secondary building unit at the truncated octahedron corners. *Inorg Chem* **2009,** *48* (4), 1281-3.

107. Wei, W.; Li, W.; Wang, X.; He, J., A Designed Three-Dimensional Porous Hydrogen-Bonding Network Based on a Metal–Organic Polyhedron. *Crystal Growth & Design* **2013,** *13* (9), 3843-3846.

108. Kim, H.; Oh, M.; Kim, D.; Park, J.; Seong, J.; Kwak, S. K.; Lah, M. S., Single crystalline hollow metal-organic frameworks: a metal-organic polyhedron single crystal as a sacrificial template. *Chem Commun (Camb)* **2015,** *51* (17), 3678-81.

109. Ma, S.; Niu, Y. F.; Zhao, X. L.; Duan, Z. M., A metal-organic polyhedron based on dibenzothiophene ligand: Gas adsorption and reductive properties. *Inorganic Chemistry Communications* **2016,** *70*, 10-13.

110. Lal, G.; Lee, S. J.; Spasyuk, D. M.; Shimizu, G. K. H., Amphiphile-like self assembly of metal organic polyhedra having both polar and non-polar groups. *Chem Commun (Camb)* **2018,** *54* (14), 1722-1725.

111. Sumida, K.; Her, J. H.; Dincă, M.; Murray, L. J.; Schloss, J. M.; Pierce, C. J.; Thompson, B. A.; FitzGerald, S. A.; Brown, C. M.; Long, J. R., Neutron Scattering and Spectroscopic Studies of Hydrogen Adsorption in $Cr_3(BTC)_2$ -a Metal-Organic Framework with Exposed Cr^{2+} Sites. *J. Phys. Chem. C* **2011,** *115*, 8414.

112. Li, J. R.; Zhou, H. C., Bridging-ligand-substitution strategy for the preparation of metal-organic polyhedra. *Nat Chem* **2010,** *2* (10), 893-8.

113. Eddaoudi, M.; Kim, J.; Wachter, J. B.; Chae, H. K.; O'Keeffe, M.; Yaghi, O. M., Porous Metal-Organic Polyhedra: 25 Å Cuboctahedron Constructed from 12 $Cu_2(CO_2)_4$ Paddle-Wheel Building Blocks. *J. Am. Chem. Soc.* **2001,** *123* (18), 4368-4369.

114. Young, M. D.; Zhang, Q.; Zhou, H.-C., Metal-Organic Polyhedra Constructed from Dinuclear Ruthenium Paddlewheels. *Inorg. Chim. Acta* **2015,** *424* (0), 216-220.

115. Li, J.-R.; Zhou, H.-C., Bridging-Ligand-Substitution Strategy for the Preparation of Metal-Organic Polyhedra. *Nat. Chem.* **2010,** *2* (10), 893-898.

116. Cotton, F. A.; Extine, M.; Rice, G. W., Sensitivity of the chromium-chromium quadruple bond in dichromium tetracarboxylates to axial coordination and changes in inductive effects. *Inorganic Chemistry* **2002,** *17* (1), 176-186.

117. Zhao, D.; Yuan, D.; Krishna, R.; van Baten, J. M.; Zhou, H.-C., Thermosensitive Gating Effect and Selective Gas Adsorption in a Porous Coordination Nanocage. *Chem. Commun.* **2010,** *46* (39), 7352-7354.

118. Murray, L. J.; Dinca, M.; Yano, J.; Chavan, S.; Bordiga, S.; Brown, C. M.; Long, J. R., Highly-Selective and Reversible O_2 Binding in Cr_3(1,3,5-Benzenetricarboxylate)$_2$. *J. Am. Chem. Soc.* **2010,** *132* (23), 7856-7857.

119. Sumida, K.; Her, J.-H.; Dincă, M.; Murray, L. J.; Schloss, J. M.; Pierce, C. J.; Thompson, B. A.; FitzGerald, S. A.; Brown, C. M.; Long, J. R., Neutron Scattering and Spectroscopic Studies of Hydrogen Adsorption in $Cr_3(BTC)_2$ -a Metal-Organic Framework with Exposed Cr^{2+} Sites. *J. Phys. Chem. C* **2011,** *115* (16), 8414-8421.

120. Bloch, E. D.; Queen, W. L.; Hudson, M. R.; Mason, J. A.; Xiao, D. J.; Murray, L. J.; Flacau, R.; Brown, C. M.; Long, J. R., Hydrogen Storage and Selective, Reversible O_2 Adsorption in a Metal-Organic Framework with Open Chromium(II) Sites. *Angew. Chem. Int. Ed.* **2016,** *55* (30), 8605-8609.

121. Sing, K. S. W., Reporting Physisorption Data for Gas/Solid Systems with Special Reference to the Determination of Surface Area and Porosity. *Pure Appl. Chem.* **1982,** *54*, 2201-2218.

122. Lu, Z.; Knobler, C. B.; Furukawa, H.; Wang, B.; Liu, G.; Yaghi, O. M., Synthesis and Structure of Chemically Stable Metal−Organic Polyhedra. *J. Am. Chem. Soc.* **2009,** *131* (35), 12532-12533.

123. Ni, Z.; Yassar, A.; Antoun, T.; Yaghi, O. M., Porous Metal−Organic Truncated Octahedron Constructed from Paddle-Wheel Squares and Terthiophene Links. *J. Am. Chem. Soc.* **2005,** *127* (37), 12752-12753.

124. Lin, K. S.; Adhikari, A. K.; Ku, C. N.; Chiang, C. L.; Kuo, H., Synthesis and characterization of porous HKUST-1 metal organic frameworks for hydrogen storage. *International Journal of Hydrogen Energy* **2012,** *37* (18), 13865-13871.

125. Peng, Y.; Srinivas, G.; Wilmer, C. E.; Eryazici, I.; Snurr, R. Q.; Hupp, J. T.; Yildirim, T.; Farha, O. K., Simultaneously high gravimetric and volumetric methane uptake characteristics of the metal–organic framework NU-111. *Chemical Communications* **2013,** *49* (29), 2992-2994.

126. Ma, S.; Sun, D.; Simmons, J. M.; Collier, C. D.; Yuan, D.; Zhou, H.-C., Metal-Organic Framework from an Anthracene Derivative Containing Nanoscopic Cages Exhibiting High Methane Uptake. *Journal of the American Chemical Society* **2008,** *130* (3), 1012-1016.

127. He, Y.; Zhou, W.; Qian, G.; Chen, B., Methane storage in metal–organic frameworks. *Chemical Society Reviews* **2014,** *43* (16), 5657-5678.

128. Wu, H.; Simmons, J. M.; Liu, Y.; Brown, C. M.; Wang, X.-S.; Ma, S.; Peterson, V. K.; Southon, P. D.; Kepert, C. J.; Zhou, H.-C.; Yildirim, T.; Zhou, W., Metal–Organic Frameworks with Exceptionally High Methane Uptake: Where and How is Methane Stored? *Chemistry – A European Journal* **2010,** *16* (17), 5205-5214.

129. Murray, L. J.; Dinca, M.; Yano, J.; Chavan, S.; Bordiga, S.; Brown, C. M.; Long, J. R., Highly-selective and reversible O_2 binding in Cr_3(1,3,5-benzenetricarboxylate)$_2$. *J Am Chem Soc* **2010,** *132* (23), 7856-7.

130. Yang, S.; Lin, X.; Lewis, W.; Suyetin, M.; Bichoutskaia, E.; Parker, J. E.; Tang, C. C.; Allan, D. R.; Rizkallah, P. J.; Hubberstey, P.; Champness, N. R.; Mark Thomas, K.; Blake, A. J.; Schröder, M., A partially interpenetrated metal–organic framework for selective hysteretic sorption of carbon dioxide. *Nat Mater* **2012,** *11* (8), 710-716.

131. Muller, K.; Wadhwa, J.; Singh Malhi, J.; Schottner, L.; Welle, A.; Schwartz, H.; Hermann, D.; Ruschewitz, U.; Heinke, L., Photoswitchable nanoporous films by loading azobenzene in metal-organic frameworks of type HKUST-1. *Chem Commun (Camb)* **2017,** *53* (57), 8070-8073.

132. Yang, Y. X.; Cao, L. Q.; Li, J.; Dong, Y.; Wang, J. D., High-Performance Composite Monolith Synthesized via HKUST-1 Stabilized HIPEs and Its Adsorptive Properties. *Macromolecular Materials and Engineering* **2018,** *303* (11), 1800426.

133. Álvarez, J. R.; Sánchez-González, E.; Pérez, E.; Schneider-Revueltas, E.; Martínez, A.; Tejeda-Cruz, A.; Islas-Jácome, A.; González-Zamora, E.; Ibarra, I. A., Structure stability of HKUST-1 towards water and ethanol and their effect on its CO_2 capture properties. *Dalton Transactions* **2017,** *46* (28), 9192-9200.

134. Anderson, J. S.; Gallagher, A. T.; Mason, J. A.; Harris, T. D., A five-coordinate heme dioxygen adduct isolated within a metal-organic framework. *J Am Chem Soc* **2014,** *136* (47), 16489-92.

135. Young, M. D.; Zhang, Q.; Zhou, H.-C., Metal–organic polyhedra constructed from dinuclear ruthenium paddlewheels. *Inorganica Chimica Acta* **2015,** *424*, 216-220.

136. Li, J.-R.; Zhou, H.-C., Bridging-ligand-substitution strategy for the preparation of metal–organic polyhedra. *Nature Chemistry* **2010,** *2*, 893.

137. Zhao, D.; Yuan, D.; Krishna, R.; van Baten, J. M.; Zhou, H. C., Thermosensitive gating effect and selective gas adsorption in a porous coordination nanocage. *Chem Commun (Camb)* **2010,** *46* (39), 7352-4.

138. Ni, Z.; Yassar, A.; Antoun, T.; Yaghi, O. M., Porous Metal–Organic Truncated Octahedron Constructed from Paddle-Wheel Squares and Terthiophene Links. *J. Am. Chem. Soc.* **2005,** *127*, 12752.

139. Lu, Z.; Knobler, C. B.; Furukawa, H.; Wang, B.; Liu, G.; Yaghi, O. M., Synthesis and Structure of Chemically Stable Metal–Organic Polyhedra. *J. Am. Chem. Soc.* **2009,** *131*, 12532.

140. Park, J.; Sun, L. B.; Chen, Y. P.; Perry, Z.; Zhou, H. C., Azobenzene-functionalized metal-organic polyhedra for the optically responsive capture and release of guest molecules. *Angew Chem Int Ed Engl* **2014,** *53* (23), 5842-6.

141. Barreda, O.; Bannwart, G.; Yap, G. P. A.; Bloch, E. D., Ligand-Based Phase Control in Porous Molecular Assemblies. *ACS Appl Mater Interfaces* **2018,** *10* (14), 11420-11424.

142. Anaya de Parrodi, C.; Walsh, P. J., All kinds of reactivity: recent breakthroughs in metal-catalyzed alkyne chemistry. *Angew Chem Int Ed Engl* **2009,** *48* (26), 4679-82.

143. Wu, Z.; Zhou, K.; Ivanov, A. V.; Yusobov, M.; Verpoort, F., The simplest and fascinating metal–organic polyhedra: Tetrahedra. *Coordination Chemistry Reviews* **2017,** *353*, 180-200.

144. Wang, Z.; Heinke, L.; Jelic, J.; Cakici, M.; Dommaschk, M.; Maurer, R. J.; Oberhofer, H.; Grosjean, S.; Herges, R.; Brase, S.; Reuter, K.; Woll, C., Photoswitching in nanoporous, crystalline solids: an experimental and theoretical study for azobenzene linkers incorporated in MOFs. *Phys Chem Chem Phys* **2015,** *17* (22), 14582-7.

145. Wang, Z.; Müller, K.; Valášek, M.; Grosjean, S.; Bräse, S.; Wöll, C.; Mayor, M.; Heinke, L., Series of Photoswitchable Azobenzene-Containing Metal–Organic

Frameworks with Variable Adsorption Switching Effect. *The Journal of Physical Chemistry C* **2018,** *122* (33), 19044-19050.

146. Larsen, R. W., How Fast Do Metal Organic Polyhedra Form in Solution? Kinetics of $[Cu_2(5\text{-OH-bdc})_2L_2]_{12}$ Formation in Methanol. *Journal of the American Chemical Society* **2008,** *130* (34), 11246-11247.

147. Rice, S. F.; Wilson, R. B.; Solomon, E. I., Electronic Absorption-Spectrum of Chromous Acetate Dihydrate and Related Binuclear Chromous Carboxylates. *Inorganic Chemistry* **1980,** *19* (11), 3425-3431.

148. Cotton, F. A.; Thompson, J. L., Dichromium(II) Compounds Containing 2-Phenylbenzoic Acid ($Biphco_2h$) - $[Cr_2(O_2cbiph)_4]_2$ and $Cr_2(O_2cbiph)_4(Thf)_2$. *Inorganic Chemistry* **1981,** *20* (4), 1292-1296.

149. Cotton, F. A.; Daniels, L. M.; Lin, C.; Murillo, C. A., Square and Triangular Arrays Based on Mo_2^{4+} and Rh_2^{4+} Units *J. Am. Chem. Soc.* **1999,** *121*, 4538.